Multi-functional liquid crystal elastomer composites

Cite as: Appl. Phys. Rev. **9**, 011301 (2022); https://doi.org/10.1063/5.0075471
Submitted: 15 October 2021 • Accepted: 26 November 2021 • Published Online: 03 January 2022

Yuchen Wang, Jiaqi Liu and Shu Yang

Applied Physics Reviews REVIEW scitation.org/journal/are

Multi-functional liquid crystal elastomer composites

Cite as: Appl. Phys. Rev. 9, 011301 (2022); doi: 10.1063/5.0075471
Submitted: 15 October 2021 · Accepted: 26 November 2021 ·
Published Online: 3 January 2022

View Online Export Citation CrossMark

Yuchen Wang, Jiaqi Liu, and Shu Yang[a]

AFFILIATIONS

Department of Materials Science and Engineering, University of Pennsylvania, 3231 Walnut Street, Philadelphia, Pennsylvania 19104, USA

[a]Author to whom correspondence should be addressed: shuyang@seas.upenn.edu

ABSTRACT

Liquid crystal elastomers (LCEs), owing to their intrinsic anisotropic property and capability of generating programmable complex morphologies under heat, have been widely used for applications ranging from soft robotics, photonic devices, cell culture, to tissue engineering. To fulfill the applications under various circumstances, high actuation efficiency, high mechanical strength, large heat and electrical conductivity, or responses to multiple stimuli are required. Therefore, design and fabrication of LCE composites are a promising strategy to enhanced physical properties and offer additional stimuli responses to the LCEs such as light, electric, and magnetic fields. In this review, we focus on recent advances in LCE composites, where LCEs are defined as anisotropic elastomeric materials in a broader context. Classic LCE composites with metallic nanoparticles, magnetic particles, liquid metal, carbon nanotubes, graphene and its derivative, and carbon black, and LCE composites from cellulose nanocrystals within the polymer network where cellulose can provide the unique liquid crystal anisotropy will be discussed. We conclude with the challenges and future research opportunities.

TABLE OF CONTENTS

I. INTRODUCTION

Liquid crystal elastomers (LCEs) of intrinsic molecular alignment can be programmed for applications ranging from soft robotics, photonic devices, biosensors, to tissue engineering. To achieve large actuation strains, LCEs should be soft, and the responses are often activated by heat near the phase transition temperatures. To broaden and enhance the properties of LCEs to achieve, for example, high actuation efficiency, high mechanical strength, and large heat and electrical conductivity, or enable responses to multiple stimuli beyond heating, a variety of strategies have been derived by integrating fillers into the LCE matrix. Depending on the nature of the fillers, LCE composites

can be photoresponsive, electro-responsive, magneto-responsive, or demonstrating multiple responses. Therefore, LCE composites are highly promising materials, which can offer new functionalities with unprecedented actuation behaviors through the synergy between the LCE matrix and the fillers.

Herein, we overview recent advances of LCE composites, where LCEs are defined as anisotropic elastomeric materials in a broader context. The topics include fillers such as metallic nanoparticles (NPs), magnetic particles, liquid metal (LM), carbon nanotubes (CNTs), graphene and its derivative, and carbon black (CB). In addition to the traditional LCE composites, LCE composites from cellulose nanocrystals (CNCs), which themselves can form lyotropic liquid crystal (LC) phases, thus offering unique assembly and anisotropy are also discussed.

In this review, the fundamental physics of LCs and LCEs in terms of alignment control, chemical nature, and phase behaviors are introduced in Sec. II. The integration and fabrication strategies of LCE composites toward programmable responsiveness and the mechanisms of responsiveness from various LCE composites systems, especially their new physical properties and functionalities compared to pure LCEs, are highlighted in Sec. III. The vast range of applications of the resulting LCE composites with unique functionalities is delved into in Sec. IV. Finally, we conclude by discussing the current challenges and future research opportunities in the field in Sec. V.

II. LIQUID CRYSTALS AND LIQUID CRYSTAL ELASTOMERS

A. Liquid crystals

LC is often referred to as the fourth state of matter that has intrinsic anisotropy, as it possesses both the fluidic property of liquid and the long-range order of crystals. LCs have been extensively studied since Friedrich Reinitzer first observed cholesteryl benzoate under the polarized optical microscope (POM) with two melting points in the nineteenth century.[1] LC molecules can self-assemble with certain orders at the micrometer level. LCs can be further categorized into thermotropic LCs and lyotropic LCs, where the formation of LC phases depends on temperature and concentration, respectively. LC molecules can have rod-like (calamitic), disc-like (discotic), or lath-like (sanidic) shapes. The long-range order in LCs leads to the most important property, that is, anisotropy, which breaks the continuous rotational symmetry. Directors align differently within domains, acting like a ferromagnet. As a result, LC is birefringent as the refractive index along the LC long axis is different from that in the perpendicular direction. Thus, light will propagate through LC at different speeds in different directions, and different LC phases can be identified by textures in POM. In addition to birefringence, dielectric property, polarization, and thermal expansion coefficients are all closely related to LC anisotropy. Molecules that exhibit LC phases are called mesogens.

1. Thermotropic liquid crystal phases

Nematic phase, smectic phase, and cholesteric phase are representative thermotropic LC phases, which may coexist depending on the temperature [Fig. 1(a)].

In a nematic phase, mesogens only exhibit one-dimensional orientational order but no positional order. All molecules tend to align along a preferred direction, which is referred to as director $\boldsymbol{n}$. Molecules are rotatable around their long axis; in other words, nematic mesogens pointing into a certain direction are regarded as equivalent to mesogens pointing

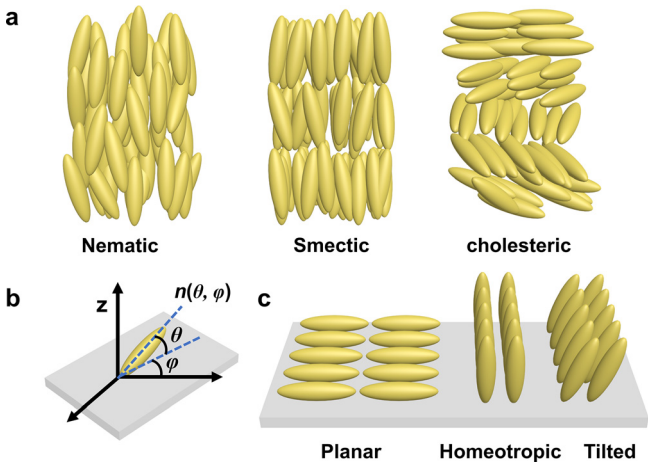

FIG. 1. (a) Schematic illustrations of typical molecular orders in thermotropic LCs. (b) Position of director $\boldsymbol{n}$ near surface is determined by polar angle θ and azimuthal angle φ. (c) The surface anchoring behaviors of LC molecules.

to the opposite direction, hence $\boldsymbol{n} = -\boldsymbol{n}$. In a smectic phase, LC mesogens exhibit one- (1D) or two-dimensional (2D) positional order with a well-defined layer structure in addition to the orientational order. In a cholesteric phase (also known as chiral nematic phase), LC mesogens containing a chiral center have the same long-range orientational order as in the nematic phase, but molecules exhibit a spontaneous helical superstructure, where molecular directors rotate periodically around the helical axis that is perpendicular to the plane. An important characteristic of the cholesteric phase is the chiral pitch, P, defined as the distance for the LC director to rotate 360°. This pitch determines the reflected wavelength of light (λ), which can be approximated by Bragg reflection[2]

$$\lambda = nP \sin \alpha, \tag{1}$$

where n is the average refractive index of the material, and α is the angle between the reflected light and the helical axis.

Although the order of LC mesogens differs locally, the average orientation of LC mesogens can be described by the order parameter S,

$$S = \int_0^{\pi} \left(1 - \frac{3}{2}\sin^2\theta\right) P(\theta) d\theta, \tag{2}$$

where θ is the angle between the director $\boldsymbol{n}$ and the long axis of a single LC molecule, and $0 < S < 1$. When $S = 1$, all mesogens align perfectly along one direction in crystals. When $S = 0$, the fluid is isotropic. S is usually between 0.4 and 0.7 for nematic LCs.

For a LC system with boundary conditions, both the free energy in bulk and surface anchoring energy should be considered to accommodate the boundary conditions.[3] The LC director fields distort, and the resulting Frank–Oseen elastic energy for distortion is determined by

$$F_{el} = \int \left\{ \frac{1}{2}K_1(\nabla \cdot n)^2 + \frac{1}{2}K_2(n \cdot \nabla \times \mathrm{n})^2 + \frac{1}{2}K_3[n \times (\nabla \times \mathrm{n})]^2 \right\} d^3r - \int \left\{ K_{24}\nabla \cdot [n \times (\nabla \times \mathrm{n}) + n(\nabla \cdot n)] \right\} d^3r, \tag{3}$$

where K_1, K_2, K_3, and K_{24} are the elastic constants of splay, twist, bend, and saddle-splay, respectively. The free energy is calculated by integration over the volume and minimized with proper boundary conditions.

When LCs are aligned on a surface, there is always a preferred direction near the surface that the LC director $\boldsymbol{n}$ follows, whose position is determined by polar angle θ and azimuthal angle φ [Fig. 1(b)]. The most common anchoring conditions are planar ($\theta = 0°$), homeotropic ($\theta = 90°$), and tilted anchoring, where the director $\boldsymbol{n}$ is oriented parallel, perpendicular, and tilted to a plane, respectively [Fig. 1(c)].

2. Lyotropic liquid crystal phases

When an anisotropic material is dispersed in a proper isotropic solvent, it can exhibit the isotropic phase at a low concentration, but phase separates into a biphasic mixture of isotropic and LC phases above a certain concentration, and finally fully form the lyotropic LC phase above the critical concentration; that is, the ordering largely depends on concentrations. The lyotropic LC phases are observed not only in geometrically anisotropic colloids such as CNCs, graphene derivatives, and CNTs, but also in bioorganisms, including DNA, tobacco mosaic virus, and some bacteria.[4] Surfactants, block copolymers, drugs, and dyes can form lyotropic LCs.

The phase transition of lyotropic LCs from the isotropic fluid to the nematic LC phase can be explained by Onsager's theory.[5,6] It assumes that individual anisotropic "colloids" (rod-like or plate-like particles) occupy different spaces, and all interactions between "colloids" are repulsive. Taking a rigid rod with length L and diameter D as an example, when the rod concentration reaches a certain level, the excluded volume of individual rods will overlap and reduce the degree of freedom, and thus, the mixing entropy decreases. To maximize the total entropy, the rods start to form orientational order to compensate for the mixing entropy loss, thus increasing the translational entropy. Therefore, the gain in orientational order above a critical concentration will lead to the formation of nematic LC phase of rigid rods, and the critical volume fraction F for nematic phase formation can be expressed by[6]

$$F \sim \frac{4L}{D}. \tag{4}$$

Although Onsager's theory is originally brought up for rod-shaped particles, the concept of excluded volume and maximizing translational entropy can be applied to plate-like ones such as graphene oxide[7] and titanium carbide $Ti_3C_2T_x$,[8] as well as surfactants,[9] and dyes.[10]

B. Liquid crystal elastomers

LCEs are lightly cross-linked polymer networks containing main-chain or side-chain LC mesogens that couple the elasticity of rubber with the anisotropic properties of LCs. Compared to isotropic hydrogels and conventional shape memory polymers (SMPs), the internal orientation of LC mesogens allows for the programmable mechanical response of LCEs by alignment control. LCEs generally have low cross-linking density and flexible polymer backbones, relatively fast stimuli-response (~100 ms)[11] with large anisotropic, and local deformations (up to 500% strain)[12] and soft elasticity[13] (i.e., non-linear response to mechanical force). The stimuli-responsive mechanical properties of LCEs can be dated back to several decades ago, when de Gennes first predicted the possibility for polymers coupled with LC to exhibit macroscopic actuation from the shape change of individually aligned polymer chains, and their ability to convert different types of energy to mechanical motion just like muscles.[14] Owing to recent advances in material chemistry and alignment techniques, LCEs have been prepared with spatial control of director fields and manipulated toward complex deformation on demand, which broadens their applications in soft robotics, photonic devices, and tissue engineering.

1. Mechanical responses of liquid crystal elastomers

LCEs undergo spontaneous and monolithic shape change driven by re-orientation of the local director field and decrease in order parameter S when transitioning from the LC phase (usually nematic phase) to the isotropic phase; that is, the network contracts along the local director and expands in the perpendicular direction, and the polymer chains adopt isotropic, spherical conformations driven by entropy. When returning to the LC phase, the polymer chains return to the elongated and aligned state, and LCEs recover to their original shapes [Fig. 2(a)].[15]

Usually, the phase transition is triggered by temperature when LCE is heated above the nematic-to-isotropic phase transition temperature (T_{NI}). The deformation of LCE networks is highly dependent on the molecular alignment of LC molecules within the structures, allowing for anisotropy in mechanical deformation, which can further amplify the deformation in-plane and induce directional shape transformation. If the LC alignment is uniform throughout the film (i.e., monodomain), shrinking occurs along the alignment direction of the LC mesogens. Hybrid alignment such as splay, twist, and cholesteric, or even more complex configurations can be applied to introduce inhomogeneity in LCEs using different alignment methods.[16–19]

In addition to the stimuli-responsive mechanical deformation of LCEs, their intrinsic anisotropy also leads to non-linear response to mechanical force, often denoted as soft elasticity.[13,20–23] For a polydomain LCE, that is, the macroscopic alignment of polymer chains is random [Fig. 2(b)], it shows a linear stress-strain relationship (elastic

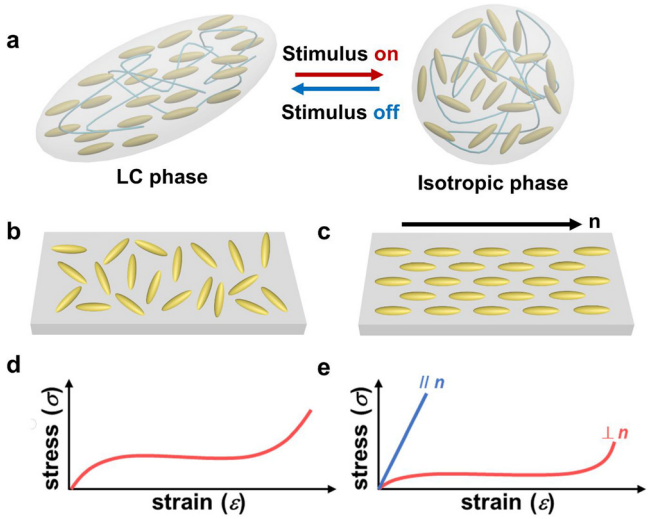

FIG. 2. (a) Schematic illustration of reversible and anisotropic shape deformation in LCE networks. (b)–(e) Polydomain and monodomain LCEs and their non-linear response (soft elasticity) subjected to mechanical stretching. (b) A polydomain LCE. (c) A monodomain LCE. Corresponding mechanical responses in (d) a polydomain LCE and (e) a monodomain LCE, where the loading direction is parallel and perpendicular to the director field, respectively.

regime) until reaching a threshold strain, where a small increase in the applied stress can lead to a large change in strain. In the plateau, the non-aligned domains will cooperatively orient along the direction of the mechanical stretching. The director field reorientation in these domains contributes to the non-linearity in the stress–strain curve. When all the domains are macroscopically aligned along the mechanical loading direction, the non-linear plateau will end. Further increase in the strain leads to strain-hardening [Fig. 2(d)]. For a monodomain LCE, that is, polymer chains align along a certain direction macroscopically [Fig. 2(c)], the stress–strain behavior is linear when the loading direction is parallel to the director field, whereas the stress–strain curve shows soft elasticity in all directions perpendicular to the director field [Fig. 2(e)].

2. Structure and chemistry of liquid crystal elastomers

LCEs can be synthesized via chemically cross-linking LC mesogens with functional groups such as thiols, acrylate, or epoxides while maintaining the liquid crystallinity. The LC mesogens can be directly attached to the polymer main chains (referred to as the main-chain LCEs) or connected to the polymer backbone via flexible spacers (referred to as the side-chain LCEs). Main-chain LCEs have stronger coupling between LC mesogens and polymer backbones; therefore, they generally exhibit superior mechanical responses compared to the side chain LCEs (Fig. 3).

The fabrication of aligned side chain LCEs was first reported by Finkelmann *et al.* [Fig. 4(a)],[24,25] where a flexible silicone-based polymer such as polymethylhydrosiloxane (PMHS) was used as the backbone, followed by hydrosilylation to incorporate reactive mesogenic monomers (RMs) and cross-linkers with vinyl groups on to the backbone. Then, the partially crosslinked soft gel was stretched uniaxially to align the polymer chains. After the residual solvent was evaporated, a second cross-linking reaction between the unreacted vinyl groups and backbone was carried out to fix the alignment. This two-step cross-linking method to achieve monodomain LCEs is based on the reaction kinetic differences between different vinyl cross-linkers. Later, polysiloxane chemistry is modified to fabricate the main-chain LCEs,[26,27] allowing for fabrication of both films and micropillars.[28]

Two-step cross-linking method has been widely adopted to prepare side chain LCEs because various LC mesogens can be chosen to react with polysiloxane. However, the difficulty to control the degree of cross-linking in different steps, the small actuation strain, and weak mechanical property compared with main-chain LCEs impedes the broader applications of this chemistry. In the past decade, two popular LCE chemistries were brought up based on chain-extension reactions with commercially available diacrylate-based RMs such as RM82 and RM257. One is the thiol-Michael addition between RMs and dithiol, multi-functional thiols, or thiol-terminated oligomers [Fig. 4(b)],[29–31] and the other is the aza-Michael addition between RM and the primary amine as the chain extender [Fig. 4(c)].[19,32]

The LCE chemistry from aza-Michael addition and thiol-Michael addition starts from a low viscosity mixture of diacrylate-based RMs and the chain extender. The low viscosity is important to ensure the effective alignment of the mixtures, which are typically infiltrated into the LC cells sandwiched between two-surface treated glass slides by capillary force. The mixture first undergoes a chain-extension reaction with amine (aza-Michael addition) or thiols (thiol-Michael addition), forming an LC oligomer. The oligomerization can also be carried out before the infiltration as long as the viscosity is low enough. Finally, the mixture is photopolymerized to fix the alignment within the cell. By adjusting the type and the ratio between the chain extender and the diacrylate mesogens, we can tune the molecular weight of the oligomers and degree of cross-linking, and hence the elasticity of LCE. The ability to synthesize and fabricate LCEs from commercially available chemicals makes it very attractive for researchers from different disciplines to manipulate LCEs for different applications.[19,29,30,33–35] However, the obtained LCEs tend to crystallize during photopolymerization of the diacrylate, which tends to homopolymerize, thus increasing viscosity and decreasing the elasticity of LCE. Therefore, efforts have been made to suppress the homopolymerization. Xia *et al.*[31] design a highly efficient LCE chemistry based on an oxygen-mediated thiol-acrylate click reaction. Thiol-terminated LC oligomers are first synthesized and then photopolymerized with diacrylate RM at a 1:1 molar ratio. In other cases, monofunctional thiols or dithiols, which act as chain transfer agents, are introduced.[34,36] The addition of non-reactive or low reactivity small-molecule thiols can also lower the viscosity. Thus, the mixture can be aligned by the surface alignment method with actuation strain up to 50% and a low glass transition temperature ($T_g < 20\,^{\circ}\mathrm{C}$). In the above LCE chemistry, the alignment and actuation mode of an obtained LCE is fixed during fabrication and cannot be reprogrammed. Therefore, there has been a growing interest in introducing dynamic covalent bonds in LCEs, where the alignment of LC mesogens can be varied after the formation of cross-linked networks, rendering LCE reprogrammable. Transesterification reaction,[37] boronic-ester exchange reaction,[38] transcarbamoylation,[39] photoexchange reactions of allyl sulfide,[40] and disulfide[41] have been introduced in LCEs. More details on LCEs with dynamic bonds or other type of backbones can be referred to the recent review articles focusing on LCE chemistry.[42–48]

3. Alignment control of the liquid crystal elastomers

To control the mechanical responses (both the magnitude and direction of the local strain), it is important to align LC molecules in local domains within the network films. There are four commonly

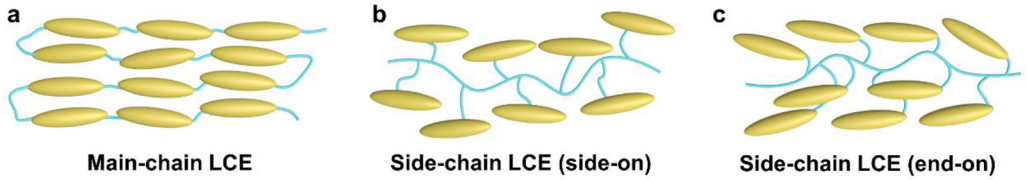

FIG. 3. Geometries for LCEs. (a) Main chain, (b) side-on side chain, and (c) end-on side chain.

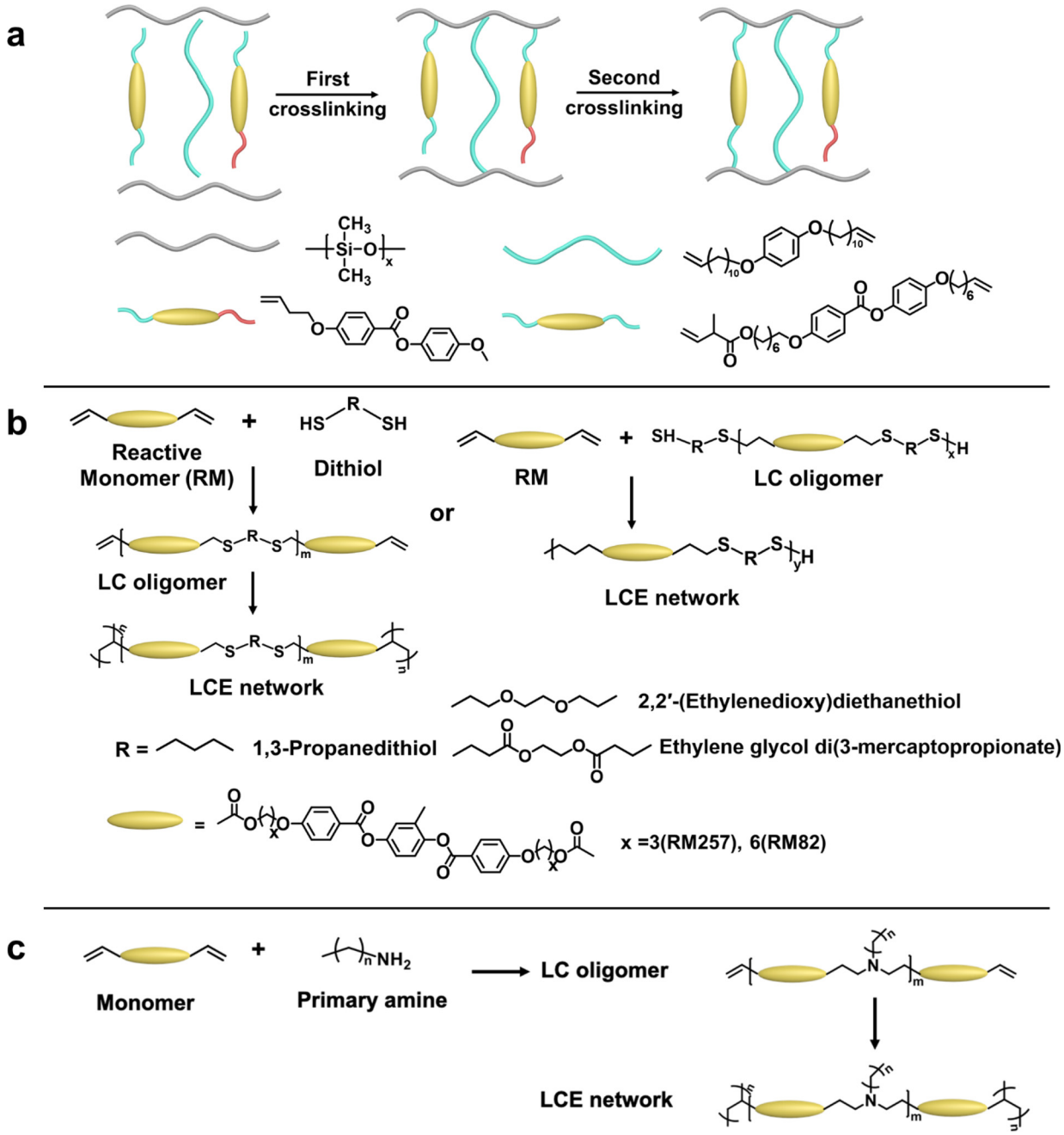

FIG. 4. Representative synthetic routes for LCE chemistry. (a) Two-step cross-linking via hydrosilylation. (b) Thiol-Michael addition between diacrylate-based RM and dithiol or RM and LC oligomer. (c) Aza-Michael addition between diacrylate-based RM and primary amine.

used alignment methods: (1) mechanical stretching, (2) surface alignment, (3) field-assisted alignment, and (4) shear alignment.

Mechanical stretching is a facile and common method to fabricate monodomain LCEs in two steps [Fig. 5(a)], where a mechanical force is applied to a partially cross-linked LCE network in the LC phase to align polymer chains along the stretching direction, followed by cross-linking under the force to lock the alignment. It has been adopted for polysiloxane based side-chain LCEs and later acrylate-based main-chain LCE thin films.[24,25,30] Recently, mechanical stretching is applied to partially cured 3D printed objects.[49] The obtained 3D actuators can exhibit a global 3D to 3D shape change rather than the uniaxial shrinkage in 2D. Since the partially cured LCEs do not have

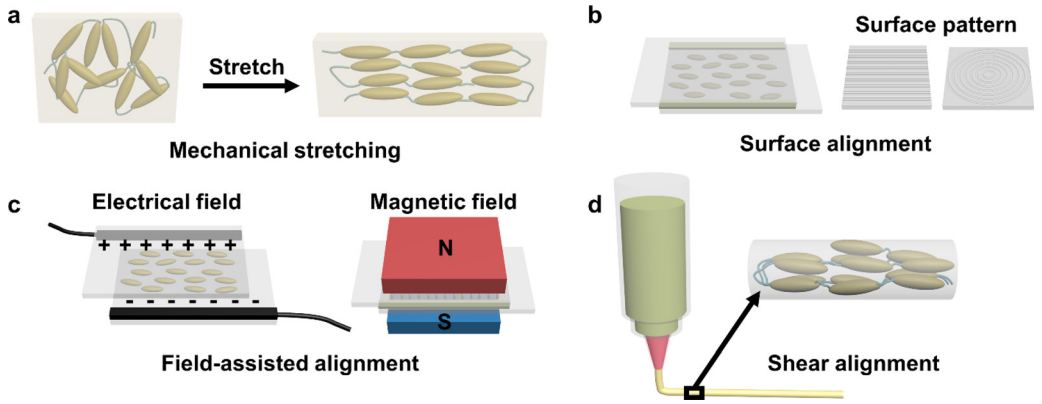

FIG. 5. Schematics of different alignment methods. (a) Mechanical stretching. (b) Surface alignment. (c) Field-assisted alignment. (d) Shear alignment.

to be aligned in the first step, that is, low viscosity is no longer a prerequisite for alignment of RM or oligomer mixtures, mechanical stretching method is the most common method to fabricate free-standing LCE composite films, consisting of gold NPs (AuNPs),[50–52] magnetic NPs,[53–55] LM,[56] and CNTs,[57–59] which often possess high viscosity. It can also help to align the nanofillers, thus enhancing anisotropy of the LCE composites. However, it is difficult to spatially control LC alignment with micrometer-scale resolution using this method.

Surface alignment is based on the interactions between LC mesogens and the substrates to minimize surface energy [Fig. 5(b)].[60] Rubbing is the standard technique in LC display industry to control alignment in a large surface area, where rubbing generates microgrooves on glass substrates coated with planar anchoring polyimide (PI) or polyvinyl alcohol (PVA). However, it is difficult to spatially control LC orientation with micrometer-scale resolution by rubbing. To realize more complex and monolithic shape change, in recent years, photoalignment and micropatterning of microchannels have been developed. In the photoalignment approach, a light-responsive material such as azobenzene-derivative is often coated on glass slides as the photoalignment layer, since azobenzene molecules exhibit angular-dependent absorption of incident light around 450 nm according to Weigert effect and can be aligned by polarized light.[61] Ware *et al.*[19] have reported voxelated local alignment in LCE films, where the topological defects guide the folding of LCE films. Photoalignment allows for alignment control within the resolution of optics, yet it is restricted to aligning LCEs in 2D films and the film thickness cannot exceed 50 μm due to finite surface anchoring energy. Because of the nature of azobenzene molecules, which gradually revert back to the *trans*-configuration under ambient light, photoalignment needs to be carried out in each new sample fabrication. Xia *et al.*[36] have used top-down techniques to fabricate microchannels to guide the alignment of LC molecules. In this approach, the dimension and orientation of channels can be arbitrarily controlled via photolithography or direct laser writing with (sub)micron resolution to minimize azimuthal angle of the LC director vs the surface, which is highly dependent on surface topography. Meanwhile, by replica molding the pattern to another material, for example, bisphenol A epoxy, which has good affinity with LCE, we minimize the zenith angle of LC director, which is highly dependent on surface chemistry. The top-down approach allows demonstration of *kirigami* folding of LCE films and realization of complex,[31] and arbitrary geometries such as a face though inverse design.[62] Surface alignment has also been applied to create LCE composites consisting of AuNPs,[63,64] magnetic particles,[65,66] and CNTs.[67] A special case of CNT/LCE composite is reported by Kim *et al.*,[68] where nanogrooves resulted from highly aligned CNTs arrays are used as the alignment layer. Although the surface alignment can spatially control LC orientations, the film thickness is usually less than 50 μm due to finite surface anchoring energy[69] and high viscosity of the composite mixture.

External fields such as electric field and magnetic field can be used to direct the LC alignment based on the anisotropic diamagnetic susceptibility and the anisotropic dielectric constant of LCs [Fig. 5(c)].[70] Compared to mechanical stretching, LC materials should have low viscosity to be aligned under an external field. Since the dielectric constant of RMs is greater along the lateral axis (negative dielectric anisotropy),[71] applying an electric field across the mesogens will induce a planar alignment. Therefore, electric field is often used together with the surface alignment to strengthen the planar anchoring.[36] However, by changing the polarity of the LCE monomers, for example, by introducing polar groups such as nitriles or esters that exhibit a positive dielectric anisotropy, it is possible to induce homeotropic anchoring.[72,73] Because of their positive diamagnetic anisotropy resulted from the aromatic rings, most RMs orient their long-axis in parallel to the applied magnetic field. Aligned micropillars that demonstrate reversible and uniaxial expansion and contraction can be obtained by applying magnetic field during soft lithography.[74,75] When the applied magnetic field is spatially oriented, more complex alignment within micropillar arrays is achieved by Yao *et al.*,[76] where they control the LC orientation in a honeycomb microstructure to realize geometry reconfiguration from buckling, shear, and transformation into a brick-wall structure. Since the dielectric anisotropy and magnetic anisotropy are typically small, a strong field is required to overcome chain mobility. In the case of LCE composites, only LCE pillars consisting of AuNPs[77] and graphene oxide[78] are reported.

3D printing techniques have been rapidly developed in recent years to fabricate delicate structures and realize shape transformation from 3D to 3D in LCEs. Photopolymerization-based 3D printing such as digital projection lithography (DLP) and two-photon polymerization (TPP) can potentially produce much higher resolution (e.g., less than 1 μm from TPP) features than direct ink writing (DIW)

techniques.[79] However, it is difficult to control LC alignment by these approaches.[80] Herein, we focus on DIW-based 3D printing of LCEs and LCE composites [Fig. 5(d)], where LC mesogens can align along the extrusion path due to the shear-thinning effect. The behavior of LC inks is well described by the Herschel–Bulkley model[81]

$$t = t_y + K\dot{g}^n, \tag{5}$$

where t is the shear stress, t_y is the yield stress, K is the consistency coefficient, $\dot{g}$ is the shear rate, and n is the flow index ($n < 1$ for shear-thinning inks). When extruded through a cylindrical nozzle, the ink experiences three zones, including an unyielded core moving with constant speed, a yielded shell with laminar flow and a thin slip layer near the nozzle wall.[82] Therefore, the ink rheology and printing conditions such as flow rate (extrusion pressure), temperature, and nozzle radius need to be fine-tuned, so that the LCs are aligned along the extrusion pathway, followed by photopolymerization to fix the alignment. LCE chemistry from both aza-Michael addition and thiol-Michael addition has been applied to DIW to realize multiple actuatable structures, including cones, helical ribbons, and grids.[83–86] When printed from multiple LCE inks, each with a characteristic T_{NI}, the obtained LCE 3D structure can demonstrate multiple and sequential folding.[86] Furthermore, the combination of LCE hinges with different T_{NI} leads to an untethered soft robot that can self-propel and shape-morph.[87] However, the alignment of each printing line is always along the printing path with relatively low resolution (the smallest width or thickness reported in literature, ~150 μm[84]). The feature size of DIW printed filament is limited by the nozzle diameter. When the nozzle diameter is greater than 1 mm, the LC alignment will be deteriorated, reducing the actuation strain almost by half.[85] Recently, 3D printing with gradient alignment within each printing line has been reported by adjusting the printing parameters such as printing at a higher temperature ($> T_{NI}$), or using a cold stage as the printing plane.[88,89] When 3D printing the LCE composite, the ink composition and printing parameters need to be adjusted accordingly, as the nanofillers can greatly alter the rheology of the ink. Currently, only 3D printing of LM/LCE has been reported.[90,91]

Depending on the target applications, we need to carefully choose the alignment method, LCE chemistry, sample dimension, and fine-tune the ink rheology. A comparison of different alignment methods is summarized in Table I.

III. LIQUID CRYSTAL ELASTOMER COMPOSITES

To improve the physical properties of the LCE such as the mechanical strength, thermal, and electrical conductivity, and promote the actuation properties such as faster speed and responses to multiple stimuli, fillers with unique optical, electrical, or magnetic properties are introduced. To obtain a robust composite, homogeneous mixing between the fillers and the LCEs is preferred. However, nanofillers are prone to aggregate due to their large surface area. In general, there are two common strategies to improve fillers' distribution in the LCE matrix. One is to chemically cross-link the fillers with the LCEs, the other is to modify the fillers with proper surface chemistry. In this section, we will discuss different strategies to embed various fillers into LCEs and the resulting properties of the composites.

TABLE I. Summary of different LCE alignment methods.

Alignment methods		Materials	Advantages	Limitations
Mechanical stretching[24,25,29,49]		■ Two-step cross-linking	■ Facile ■ Scalable	■ Not capable of local alignment with micrometer-scale resolution
Field-assisted alignment	■ Electric field[72,73]	■ Low viscosity side-chain RMs and oligomers	■ Applicable for homeotropic alignment ■ Applicable for 3D microstructures such as micropillars	■ Difficult for large-scale fabrications
	■ Magnetic field[74-76,92–95]			
Surface alignment	■ Rubbing[96]	■ Low viscosity side-chain RMs;	■ Facile	■ Not capable of local alignment with micrometer-scale resolution
	■ Photoalignment[19,97]	■ main-chain RMs and oligomers, based on chain-extension reactions	■ Spatial control of the alignment with micrometer-scale resolution	■ Relatively low viscosity of resin required; ■ Film thickness $\leq$ 100 μm
	■ Patterned microchannels[31,62,98]			
Shear alignment (e.g., Direct-ink-writing)[83–89]		■ Main-chain RMs, based on chain-extension reactions	■ Facile alignment along the printing path in arbitrary shapes	■ Alignment along the printing path; ■ Need to consider ink rheology; ■ Feature size limited by the nozzle size

A. LCE composites with fillers

1. Photothermal metallic nanoparticles

Photothermal metallic NPs, such as gold and silver, have been of great interest due to their unique optical properties resulted from the localized surface plasmon resonance (LSPR). Metals are known to have a sea of electrons. When the particle size is at the same length order of magnitude of the incoming electromagnetic wavelength, the electric field can cause the electrons to oscillate coherently. The resultant oscillation can generate a huge amount of heat due to mass collision between the electrons and phonons. This is known as the photothermal effect. Thus, metallic NPs can be the fillers to not only enhance the mechanical property of the LCEs, but also provide LCEs with the remote and localized light response, where the actuation light wavelength can be well controlled by the size and the shape of the photothermal metallic NPs.

Great efforts have been made in fabricating AuNP/LCE composites, due to chemical stability and a wide variety of morphologies of AuNPs that can be achieved. Montazami *et al.*[63] fabricate AuNP/LCE and find that both Young's modulus, thermal conductivity, and response speed of the composites are greatly improved with only 0.096 mol. % AuNP embedded. Sun *et al.*[99] fabricate AuNP/LCE pillars using a molding technique under a strong magnetic field. The resulting AuNP/LCE actuators can be spatially translated, aligned, and rotated by polarized-light optical tweezers. Liu *et al.*[77] incorporate both gold nanosphere (AuNS) and gold nanorod (AuNR) into LCEs, and the AuNR/LCE composites achieve 30% actuation strain upon irradiation of a 635 nm laser with less than 1 wt. % AuNRs. However, aggregation of the AuNPs weakens the performance of the composites.

Therefore, proper LCE chemistry, fabrication method, and surface modification of the AuNPs should be considered. Strong Au-S bonds can be utilized to improve the compatibility between the AuNPs and LCE.[100] Yang *et al.*[52] successfully fabricate AuNR/LCE fibers via three-step thiol-ene click chemistry. First, ∼70 mol. % thiol groups from poly(3-mercaptopropylmethylsiloxane) (PMMS) react with mesogenic alkene, forming PMMS-*g*-LC. When mixing with AuNRs, the unreacted thiol groups bond with AuNRs. In the third step, the remaining thiols on PMMS-*g*-AuNRs are mixed with triallyl cyanurate and pulled to create aligned AuNR/LCE fibers, followed by UV exposure to lock the alignment [Fig. 6(a)]. With 0.09 wt. % loading of AuNRs, the AuNR/LCE fibers shrink ∼30% under 808 nm laser. Wojcik *et al.*[51] also cross-link AuNPs with LCE by modifying AuNPs with thiol-terminated mesogenic olefin ligands, followed by cross-linking with PMHS through the C=C bond on the ligand.

AuNPs with proper surface modification can be also directly mixed with LCEs. For example, Xu *et al.*[50] modify AuNPs and fabricate side-chain AuNP/LCE by immersing the partially cross-linked LCE into a AuNP/toluene solution. The resulting composites show 30% actuation upon irradiation with a solar light source (4.0×10^5 lux). We functionalize AuNRs with thiol-terminated poly (ethylene glycol) (PEG-SH) and successfully fabricate AuNR/LCE film with excellent photothermal performance.[64] In this case, LC oligomers are first synthesized through thiol-Michael addition using 1,3-propanedithiol and RM82 at 2:1 molar ratio. The oligomerization process significantly reduces the reactivity of the thiol groups on the oligomers for Au surface, but making the PEG-modified AuNRs compatible with the LCE precursor consists of oligomers and monomers RM82 [Fig. 6(b)]. The resulting AuNR/LCE films with 0.20 wt. % AuNRs show a better mechanical property and can reach 149.5 °C under the exposure of 800 nm light within 5 s, at 784 mW cm^{-2}. This method offers an effective and convenient approach to combine AuNPs with thiol-acrylate LCE chemistry. In addition, it is also possible to fabricate AuNP/LCE by *in situ* reduction of Au salt. For example, Kuenstler *et al.*[101] swell LCE films in a toluene solution containing $HAuCl_4$ and a reducing agent. When exposed to light, AuNPs are formed and can be locally patterned within the LCE [Fig. 6(c)].

In addition to AuNPs, other metallic NPs such as silver, copper, and nickel also have photothermal effects. However, most types of literature are reported from AuNPs, possibly due to the incompatibility and instability of other NPs in the LCEs.[102,103] Meanwhile, compared with the isotopic nanospheres, anisotropic NPs offer higher photothermal efficiency and better LSPR tunability, although they may suffer from both aggregations and reshaping, especially when operating at high temperatures. Therefore, increasing the compatibility between the metallic NPs and LCE is still a major challenge.

2. Magnetic particles

Magnetic NPs and microparticles have also been introduced to endow LCEs with magnetic responses. Magnetic NPs are also known to generate heat under the alternating electromagnetic field through the hysteresis loss and relaxation processes.[104] Similar to metallic NPs, chemical cross-linking of the particles within the LCEs can offer stable and robust composites. Song *et al.*[105] fabricate side-chain Fe_4O_3/LCE composites by covalent attachment of the LC molecules to oxide surfaces. In a typical procedure, Fe_4O_3 NPs are first functionalized with dopamine. Then, the dopamine-modified Fe_4O_3 nanoparticles and LC mesogens are bonded to the siloxane backbones [Fig. 7(a)]. Garcia-Marquez *et al.*[106] fabricate main-chain Fe_4O_3/LCE composites by modifying the Fe_4O_3 NPs with 4-undec-10-enoxybenzoic acid. Then, the double bonds on the Fe_4O_3 NPs are further cross-linked with the LC monomers. Haberl *et al.*[53,107] synthesize α-Fe_2O_3-based ellipsoidal core-shell NPs, where the silica shell is functionalized with amine groups. The hydroxyl groups from the LCE and amino groups from the NPs can be cross-linked with tri-functional isocyanate. The resulting composite show magnetic memory that can be reversibly stored by mechanical deformation and erased by heating to moderate temperatures (80 °C) [Fig. 7(b)]. Cmok *et al.*[108] attach methacrylic anhydride to ricinoleic acid on the surface of the barium hexaferrite ($BaFe_{12}O_{19}$) and then cross-link $BaFe_{12}O_{19}$ with the LC oligomer synthesized by aza-Michael addition.

Magnetic NPs can be also directly mixed with LCEs. For example, Kaiser *et al.*[54] and Winkler *et al.*[55] successfully fabricate side-chain Fe_3O_4/LCE composites using N-oleoylsarcosine as the ligand to stabilize Fe_3O_4, achieving up to 30% reversible contraction under the magnetic field. Other ligands, such as lauric acid and oleic acid, modified Fe_3O_4 NPs, and cobalt nanorods LCE composites are also reported.[109,110] Recently, Ditter *et al.*[111] modify Fe_3O_4 NPs with poly(methyl methacrylate-*b*-dopamine acrylamide) P(MMA-*b*-DOPA) block copolymers through strong bonds between the catechol groups on the dopamine and the oxidic surfaces. The resulting main-chain Fe_3O_4/LCE composites show 30% reversible actuation under ambient heat and 20% reversible actuation under light when

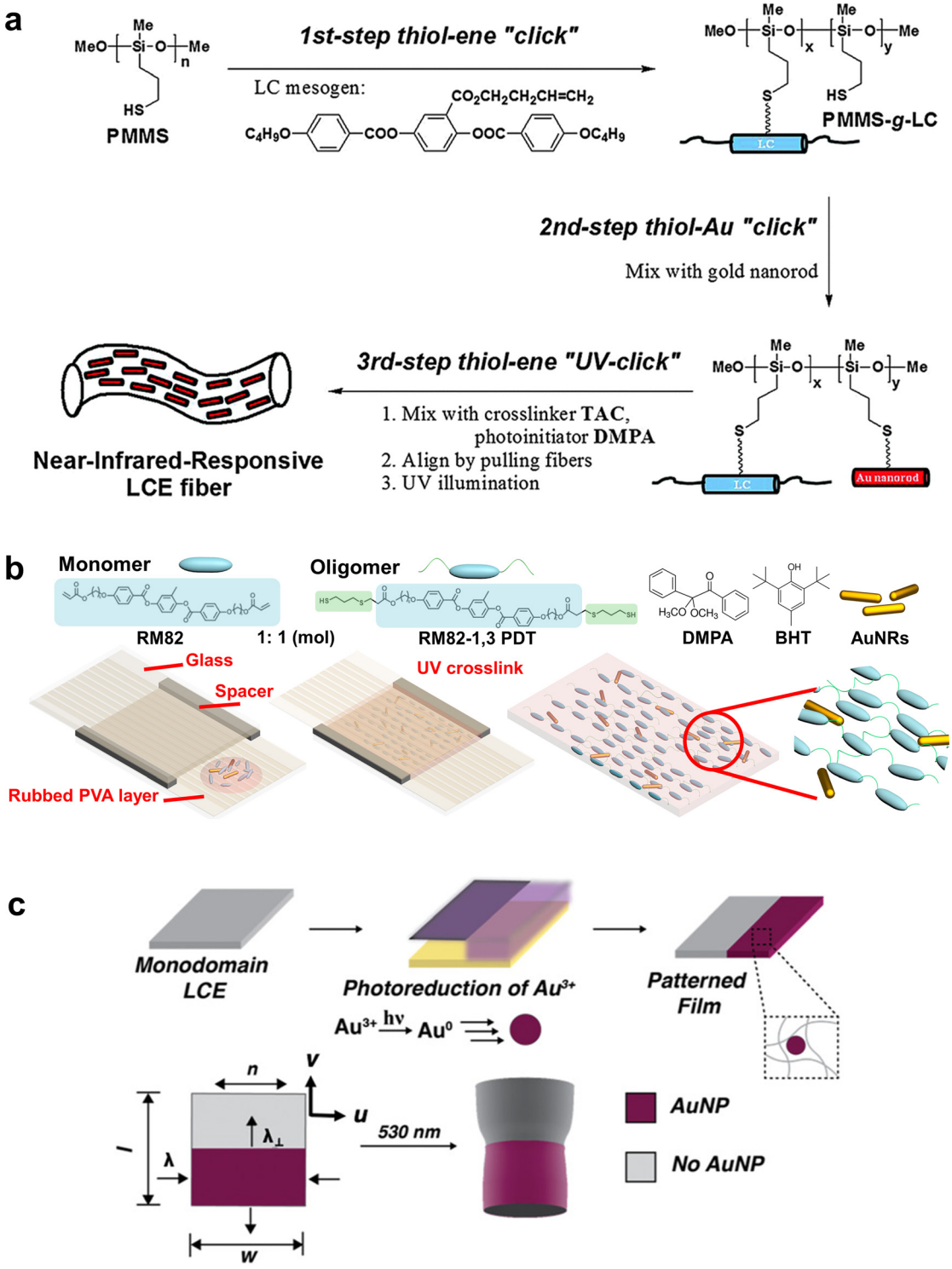

FIG. 6. Fabrication of AuNP/LCE composites. (a) Schematic of a three-step sequential thiol-click chemistry approach to prepare AuNR/LCE composites.[52] Reproduced with permission from Yang *et al.*, Chem. Commun. **51**, 12126 (2015). Copyright 2015 RSC. (b) Schematic of the steps to fabricate AuNR/LCE films.[64] Reproduced with permission from Wang *et al.*, Adv. Mater. **32**, 2004270 (2020). Copyright 2020 Wiley-VCH. (c) Photopatterning of AuNP/LCE. AuNPs are spatially incorporated into LCEs via photoreduction of gold salt with UV light.[101] Reproduced with permission from Kuenstler *et al.*, Adv. Mater. **32,** 2000609 (2020). Copyright 2020 Wiley-VCH.

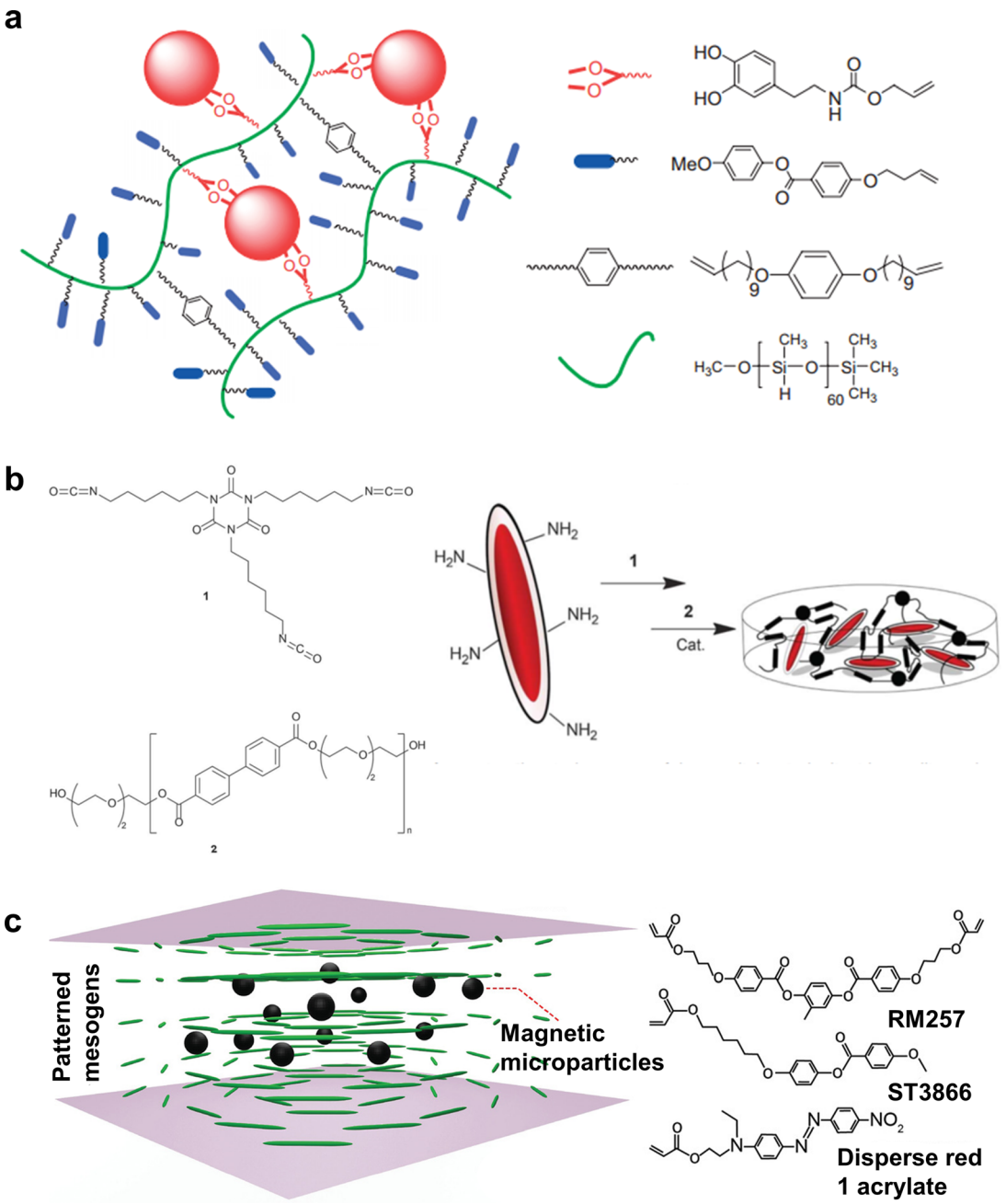

FIG. 7. Fabrication of magnetically responsive LCE composites. (a) Schematic illustration of the ferrite/LCE composites. Nematic LCs and dopamine-modified Fe_4O_3 nanoparticles are covalently bonded to the siloxane network.[105] Reproduced with permission from Song *et al.*, Adv. Funct. Mater. **17**, 2070 (2007). Copyright 2007 Wiley-VCH. (b) Solution casting of LCE composite consisting of the magnetic core-shell ellipsoidal nanoparticles.[101] 1: cross-linker and 2: LCE. Reproduced with permission from Haberl *et al.*, Nanoscale **5,** 5539 (2013). Copyright 2013 RSC. (c) Magnetic LCE composite film embedded with magnetic microparticles for programmable and multiple degree-of-freedom shape-morphing.[65] Reproduced with permission from Zhang *et al.*, Adv. Mater. **33,** 2006191 (2021). Copyright 2021 Wiley-VCH.

azobenzene LCEs are used. They can also be guided to move in water by external magnetic fields.

Compared with NPs, microparticles are more stable, where a small degree of aggregation may not affect the overall magnetic property of the composites. Zhang *et al.*[65] embed up to 24 vol. % 5 μm NdFeB microparticles into the main-chain LCE [Fig. 7(c)] to realize different locomotion modes. However, the microparticle composites usually have smaller actuation strains compared with the NP

composites, because of the increased Young's modulus (up to ten times)[66] resulting from higher loading of microparticles [50 wt. % (Refs. 65 and 66) vs less than 7 wt. % NPs[53,111]] to achieve consistent and controllable magnetic response.

Although various magnetic LCE composites have been successfully fabricated for different applications, compatibility between the particles and the LCE remains the main challenge and different types of magnetic particles are needed for specific applications. For example, for magnetic field-induced heating, magnetic particles with high thermal magnetic efficiency are required. For information storage, magnetic particles with precise and fast response to the magnetic field, high stability after the response, yet rewritable to remove the memory will be highly desired.

3. Liquid metal

LM is a metal or a metal alloy in the liquid state at room temperature. The alloys of eutectic gallium indium (EGaIn) have caught a great deal of attention because of their low toxicity, low melting point, and high conductivity. Therefore, they have been widely investigated for wearable electronics, self-healing devices, and actuators.[112] LM can enhance the electrical and thermal conductivity of the LCEs and offer LCEs with electrical response through Joule heating. Due to the intrinsic soft nature of the LM, the LM/LCE composite can also be compliant and deformable. However, it is challenging to integrate LM within LCE due to the extremely high surface tension (640 mN m^{-1}) of LM, which forms near-spherical droplets in the polymer matrix.

It is possible to incorporate LM emulsions with LCE. For example, Ford *et al.*[56] fabricate LM/LCE with up to 50 vol. % LM microparticles (~200 to 500 μm), demonstrating sensing, actuation, circuitry, and soft robot locomotion. The LM is first mixed with the RM257, tetra-functional thiol cross-linker, di-functional thiol spacer. After the first stage thiol-Michael addition, the LM/LCE is mechanically stretched and cross-linked [Fig. 8(a)]. Smaller LM particles can increase the elastic modulus from 0.3 to 4.3 MPa but decrease the actuation strain from 50% to 5% under 70 kPa load.[113] Ambulo *et al.*[90] 3D print LM/LCE composite, where the LM/LCE. The ink is obtained by mixing the LM with LC oligomers prepared through aza-Michael addition between RM257 and n-butylamine. During the mixing, acetone is added to lower the viscosity of the ink and facilitate LM dispersion [Fig. 8(b)]. The 3D printed LM/LCE actuators show reversible actuation through Joule heating and photothermal heating without dramatically increasing elastic modulus.

Although successful examples of integration between LM and LCEs have been reported, advantages of LM such as self-sensing and self-healing properties are not fully utilized. To address these properties, Ma *et al.*[114] mix LM with magnetic microparticles and control the flow of the LM on the LCE by a magnet to form an LM circuit, where LCE is covered by a channel patterned tape. After encapsulated by silicone, the resulting composite can be utilized as an actuator and a sensory skin to perceive its deformation. Kent *et al.*[115] fabricate LM/LCE composites with fluidic channels of LM. The LCE layer is first sprayed with LM microparticles and then ablated into desired channel pattern by a UV laser, followed by encapsulation with another layer of LCE. The composite can be used as a heating element and a sensor for tracking positions. Kotikian *et al.*[91] 3D print core-shell LM/LCE via co-extrusion of LM and LC oligomers, leading to the formation of pure LM core within LCE-based coaxial fibers [Fig. 8(c)]. Programmable actuation, self-sensing, and closed-loop control with up to 50% strain are demonstrated.

Direct mixing of LM emulsions with LC monomers or LC oligomers is not preferred for applications such as self-sensing and self-healing, where connectivity and conductivity of LM/LCE composites are important to the change of resistance upon deformation. Unless one can greatly reduce the surface energy of LM, which is known for the intrinsically high surface energy, it is impossible to obtain a homogenous mixture of LM and LCE.

4. Carbon nanotubes

CNTs are tubular nanostructures that consist of a hexagonal arrangement of carbons. Single-wall carbon nanotubes (SWCNTs) can be ideally regarded as a single sheet of graphene that is rolled up, while the multi-wall carbon nanotubes (MWCNTs) consist of serval layers SWCNTs weakly bound together by van der Waals interactions. CNTs offer high electric (10^6 S/m)[116] and thermal conductivity (>3000 W/m K)[117] due to a large number of mobile π-electrons along the long axis, and excellent mechanical properties (Young's modulus ~1 TPa)[118] due to interlocking C-C covalent bonds. They also have photothermal effects. Importantly, they can be modified by covalent attachment of chemical groups through reactions on the conjugated skeleton of CNTs, or by the noncovalent supramolecular adsorption or wrapping of various functional molecules onto the tubes.[119] Therefore, CNTs can be coupled with LCEs to improve the mechanical, electrical, and thermal conductivity of the LCEs. CNT/LCE composites can be also actuated by electricity through either Joule heating[68] or unique dielectric responses[67] for applications such as soft robotics.[120] If the alignment of the CNTs can be controlled, the intrinsic anisotropy of the CNTs can be couple with LCEs.

Courty *et al.*[121] report the first side-chain polysiloxane-based CNT/LCE composite fabricated through a two-step method with a maximum loading of 0.02 wt. % SWCNTs. The SWCNTs are found to be aligned with LCE during the mechanical stretching process, leading to an increase in Young's modulus from 0.75 to 1.2 MPa. Even at such a low loading, a significant electromechanical effect is observed. The dielectric torque generated by CNTs can result in uniaxial mechanical stress of 1 kPa under ~1 MV/m of direct current (DC). Ahir *et al.*[59] demonstrate the infrared actuation behavior of the CNT/LCE composite later using a similar method. However, the major challenge is to achieve higher CNTs loading in LCEs without significant aggregation. Chambers *et al.*[122,123] swell LCEs using a CNT/toluene solution, where CNTs can be absorbed onto LCE through the van der Waals attraction and form a conducting layer. However, the loading is low and hard to control. More importantly, CNTs mostly concentrate on the surface of LCE, forming a 2–3 μm CNT layer rather than being incorporated homogeneously into the LCE matrix.

To tackle this problem, Chen *et al.*[124] propose a noncovalent functionalization approach to tailor the CNT property without affecting their intrinsic properties. Poly(aryleneethynylene) (PPE) is used to solubilize the CNTs through π–π stacking, which allows control over the distance between functional groups on the CNT surface by varying the polymer backbone and side chains. Therefore, PPE-modified SWCNTs have been applied to achieve homogeneous dispersion in the polymer matrix. Yang *et al.*[57] fabricate a side-chain SWCNT/LCE

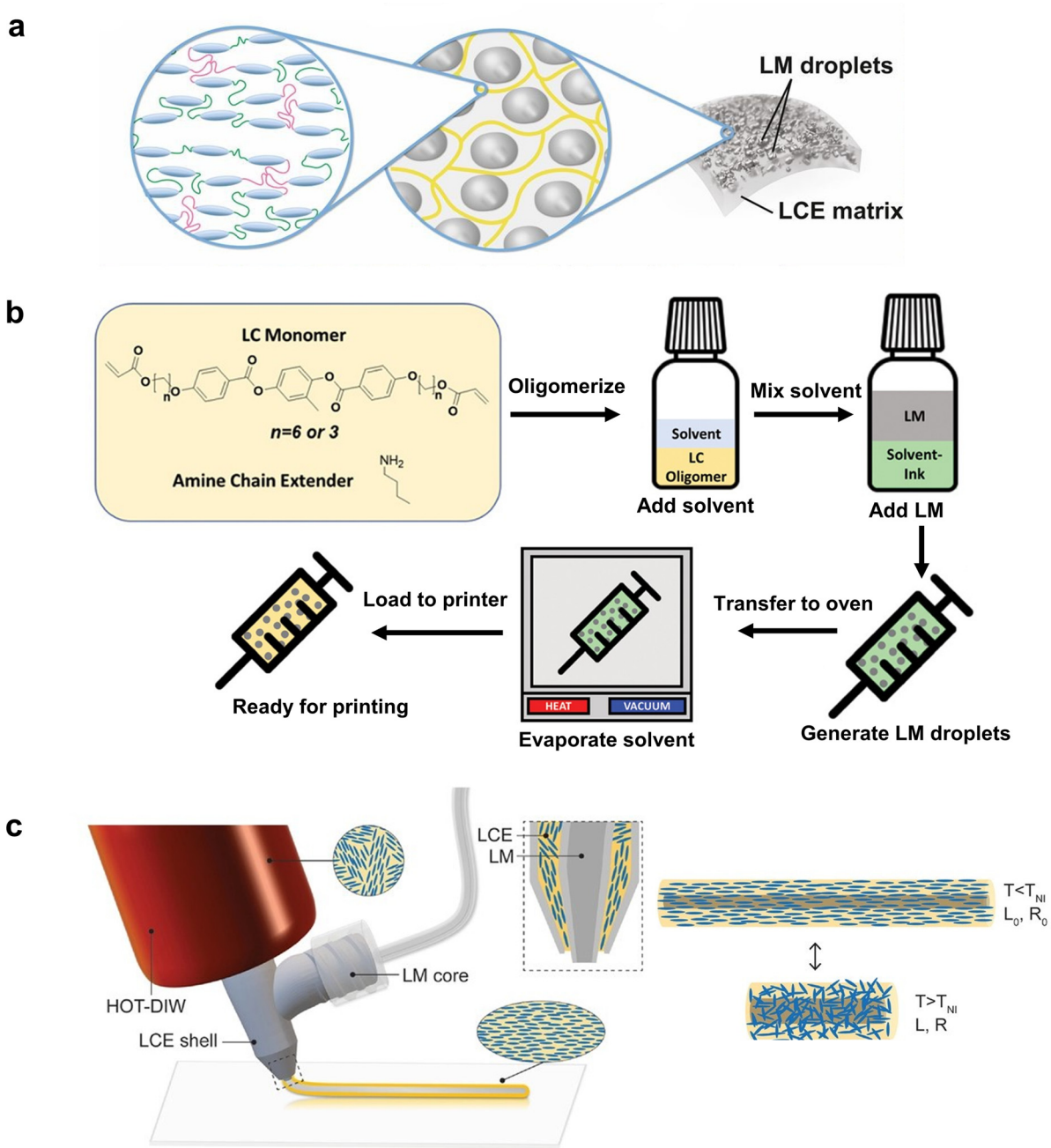

FIG. 8. Fabrication of LM/LCE composites. (a) Illustrations of the molecular, microscale, and mesoscale ordering of LM-LCE composites.[56] Reproduced with permission from Ford *et al.*, Proc. Natl. Acad. Sci. U. S. A. **116**, 21438 (2019). Copyright 2019 National Academy of Sciences. (b) The procedures to generate the printable ink from acrylate-terminated LM/LC oligomers.[90] Reproduced with permission from Ambulo *et al.*, ACS Appl. Mater. Interfaces **13**, 12805 (2021). Copyright 2021 ACS. (c) Schematic illustration of 3D printing of the innervated LM/LCE fibers composed of LM core surrounded by LCE shell and the corresponding actuation when cycled above and below the T_{NI}.[91] Reproduced with permission from Kotikian *et al.*, Adv. Mater. **33**, 2101814 (2021). Copyright 2021 Wiley-VCH.

composite with 0.2 wt. % SWCNT through a "hot-drawing" technique. The LCE precursor and PPE-SWCNTs are mixed in chloroform. Then, a film is cast, vacuum-dried, heated on a hot plate, and partially polymerized. Finally, the film is photopolymerized under uniaxial stress. The excellent dispersion of PPE-SWCNT in the LCE matrix provides a 30% reversible IR-induced strain with only 0.1 to 0.2 wt. % SWCNT loading. Ji *et al.*[125] introduce pyrene moieties at the ends of the main-chain LCEs to enhance the stability between the CNTs and

LCE through π–π stacking. Up to 3 wt. % CNTs are successfully loaded into pyrene contained LCE, showing excellent IR actuation and improvement in dielectric response [Fig. 9(a)]. Li *et al.*[126] also report side-chain SWCNT/LCE fabricated by the hot-drawing process. The resulting SWCNT/LCE nanocomposites can not only be actuated by IR light but also by a much wider spectrum of light with an intensity of 100 mW cm^{-2}. Interestingly, adding SWCNTs can also lower the T_{NI} of the LCE,[127,128] although the reason remains unclear.

Compared with side-chain chemistry, main-chain mesogenic monomers are reported to act as mild dispersants to prevent CNTs from aggregation.[129,130] Guin *et al.*[67] successfully fabricate SWCNT/LCE composites using thiol-Michael addition chemistry through the photoalignment. A maximum loading of 0.08 wt. % SWCNTs is achieved due to the increased viscosity. The resulting composites can undergo a spontaneous and reversible shape change under DC. They further fabricate SWCNT/LCE composite with 1 wt. % SWCNTs that can contract over 4% against a 140 kPa load using mechanical stretching method.[131] We fabricate CNT/LCE filaments with up to 2 wt. % CNTs in the LCE matrix by extrusion.[120] To increase the shearing force during the extrusion, up to 4 wt. % cellulose nanocrystals are added. The resulting CNT/LCE composite filaments exhibit enhanced mechanical robustness and faster actuation speed with a maximum work capacity of 38 J kg^{-1} [Fig. 9(b)]. Highly aligned CNT arrays drawn from the CNT forest can also act as the alignment layer for small LC molecules by the anisotropic nanogrooves. Kim *et al.*[68] capillary infiltrate the mixture of LC monomers and cross-linkers into a cell coated with forest-drawn CNTs, followed by cross-linking in the aligned nematic state. By controlling the orientation, location, and quantity of layers of CNTs, the resulting film can be actuated by visible light or electrical current rapidly (within 1.2 s under 280 mW cm^{-2} light) [Fig. 9(c)].

The CNT/LCE composite could become a conductor when the loading of CNTs is above the percolation threshold (typically 0.03 to 5 wt. %, depending on the size and nature of the CNTs and the type of the polymer matrix).[132] However, CNT/LCE with 3 wt. % CNTs (diameter 60–100 nm, length 5–15 μm) is not electrically conductive.[125] Also, due to the high Young's modulus of CNTs, one needs to balance between the light intensity or electrical power needed and the mobility nature of mesogens in the polymer network. The anisotropic coupling between the CNTs and LCEs has been demonstrated with the CNTs aligned along with the LCE directors.[57] It will be interesting to see whether the alignment of CNTs and LCEs can be controlled separately so that composites with new and controllable anisotropic properties can be realized to enhance the actuation performance.

5. Graphene and its derivatives

Graphene is another allotrope of carbon consisting of a single layer of atoms arranged in a two-dimensional honeycomb lattice. Similar to CNTs, graphene exhibits many superior properties, such as

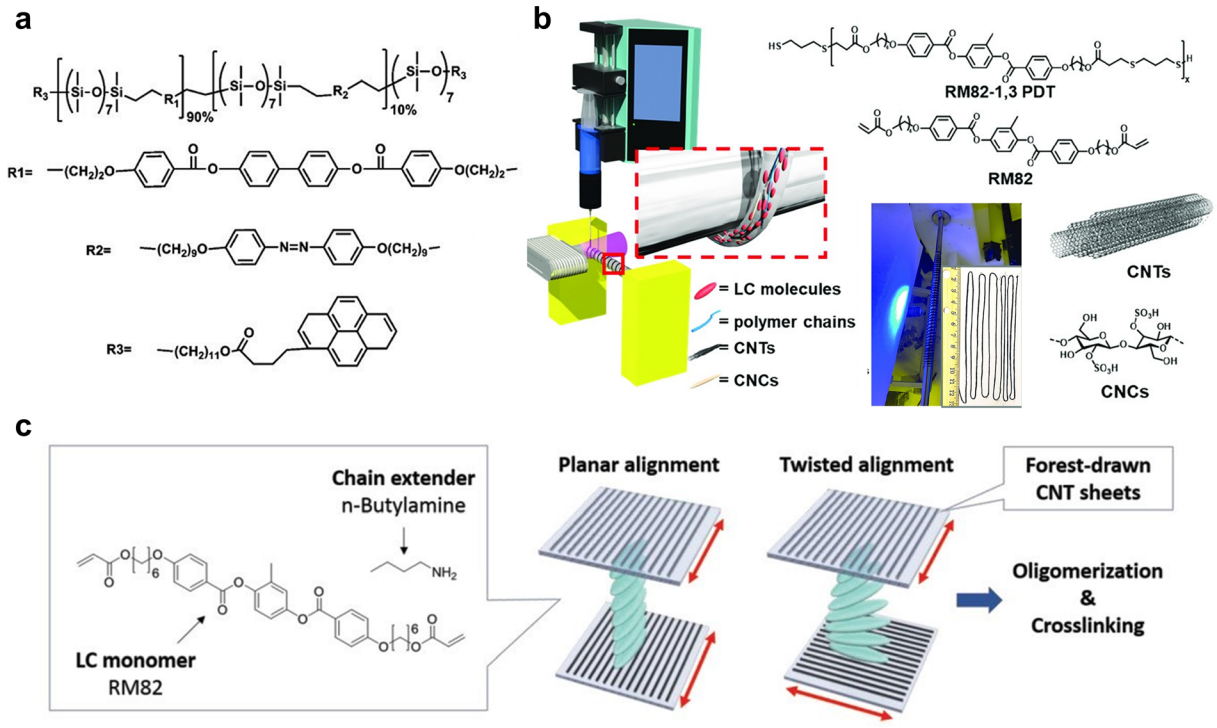

FIG. 9. Fabrication of CNT/LCE composites. (a) Chemical structure and components of the pyrene main-chain copolymer to stabilize the CNTs.[125] Reproduced with permission from Ji *et al.*, Adv. Mater. **22**, 3436 (2010). Copyright 2010 Wiley-VCH. (b) Fabrication of CNT/LCE composite filaments and their digital images. Inset: a 1.4-m-long filament.[120] Reproduced with permission from Liu *et al.*, Adv. Intell. Syst. **2**, 1900163 (2020). Copyright 2020 Wiley-VCH. (c) Fabrication of CNT/LCE composite films, where the highly aligned, forest-drawn CNT sheets are used to direct the alignment.[68] Reproduced with permission from Kim *et al.*, Adv. Funct. Mater. **29**, 1905063 (2019). Copyright 2019 Wiley-VCH.

its fantastic mechanical strength (Young's modulus, ∼1 TPa),[133] unparalleled thermal conductivity (∼5000 W/m K),[134] charge carriers mobility (200 000 cm^2/V s) properties,[135] and superior photothermal effect.[136] However, due to the hydrophobic nature, its derivatives, graphene oxide (GO) and reduced graphene oxide (rGO), are typically used in polymer composites systems. GO is the oxidized form of graphene with various oxygen-containing functionalities such as epoxide, carbonyl, carboxyl, and hydroxyl groups, making it less conductive. To increase thermal and electrical conductivity, GO is typically subjected to chemical or thermal reduction process to form rGO with less oxygen content.[137] The different properties of GO and rGO can be related to their carbon–oxygen ratio. The smaller the carbon–oxygen ratio, the better the conductivity, the higher surface area, and the stronger mechanical strength, although it also reduces hydrophilicity. Additionally, the richness of chemical groups on GO can be further utilized for functionalization. It suggests that one can engineer the structure of the GO to meet the requirement for different applications.

Graphene sheets and LCE mixtures can form stable suspensions through the π–π stacking between graphene and aromatic rings on LC mesogens. In addition, the hydroxyl and carboxyl groups in GO can form hydrogen bonding with the ester groups in the mesogens. Li *et al.*[138] report a GO/LCE with 0.7 wt. % GO loading, showing 33% reversible contraction under the white light (∼100 mW/cm^2), a ∼50% increase compared with the pure LCE. Wei *et al.*[78] modify GO with the mesogenic groups and fabricate GO/LCE micropillars by soft lithography using magnetic alignment, showing 30% thermal actuation strain and light responses. It would be beneficial if the GO can be also aligned with the LCE. Yang *et al.*[139] report an aligned rGO/LCE composite for tunable photomechanical actuation through the hot-drawing process. Large contraction strain (35.7%), high actuation stress (240 kPa), and fast response (8 s) are achieved with only 0.2 wt. % rGO as the enhanced sp^2-hybridization due to reduction and mechanically induced alignment of rGO in LCEs.

Despite extensive studies, the loading of GO remains low, less than 1 wt. %.[138,139] Current research mostly focuses on the mechanical property and the photothermal actuation, yet the electrical conductivity and actuation are less studied.

6. Carbon black

Conductive CB particles can be also doped into LCEs for electrothermal actuation based on the Joule heating effect. Wang *et al.*[140] directly mix 2 wt. % CB in toluene with LCE precursors to improve the thermal conductivity. Chamber *et al.*[141] swell the cross-linked LCE network with a CB toluene solution, achieving reversible actuation up to 150%. Agrawal *et al.*[142] introduce CB particles into the LCE network both before and after the network formation by immersing it into a CB particle toluene solution for additional doping near the surface. By this two-step doping method, they realized resistivity lower than 10 Ω m with only 6 wt. % CB. In general, increasing CB concentration can effectively improve the thermal conductivity and electric conductivity; however, it will compromise LCE actuation strain.[140–143]

7. Other nanoparticles

Other fillers, including ferroelectric ceramic nanoparticle and conductive molybdenum-oxide nanowires, have also been incorporated into the LCE matrix. For example, Domenici *et al.* embed 5 wt. % ferroelectric $PbTiO_3$[144] and 1 wt. % molybdenum oxide[145] in the side-chain LCE using the two-step method. The resulting composites show reversible actuation but smaller actuation strain (∼10% less compared with pure LCEs). In fact, many fillers with special optical, electrical, or magnetic properties can be introduced into LCEs to promote response speed and sensitivity to multiple stimuli (see summary in Table II).

B. LCE composites from LC-phased cellulose derivatives

Biomass such as cellulose fibrils can be obtained from abundant natural sources, including plants, bacteria, and fungi [Fig. 10(a)]. Cellulose fibrils consist of both amorphous and crystalline regions, where the crystalline regions can be separated by acid hydrolysis to obtain rod-like cellulose nanocrystals (CNCs). Sulfuric acid is commonly used to extract CNCs, leaving negatively charged sulfate half ester surface functional groups on CNCs [Fig. 10(b)] to a stable dispersion. The hydrolysis conditions and the source of cellulose fibrils play important roles in the aspect ratio, polydispersity, and surface charges of the obtained CNCs, which affect not only the colloidal suspension stability, but also their ability to self-assemble into the lyotropic LC phases. The dimensions of CNCs expand from 50 to 1160 nm in length and from 3 to 50 nm in width, and their chirality originated from the 1,4-D-glucose units can lead to the formation of helical superstructures, that is, the cholesteric LC phase[2,157] that always has left-handed helical twist.[157] The distance between two layers along the helical axis where the CNCs adopt the same orientation after a 360° rotation is usually defined as helical pitch, P. When light propagates through this birefringent cholesteric phase, it leads to reflection of left-handed circular polarized light [Fig. 10(c)], and the reflected wavelength λ can be approximated by that from Bragg reflection.[2] Since the reflected light is always left-handed, the maximum achievable reflectance is 50%. When the reflected wavelength falls into the visible region, the reflected light can be observed by naked eyes as structural color. Therefore, CNCs have been extensively explored for their potentials as photonic crystals to reflect light.

The self-assembled helical structures in CNCs can be fixed by evaporating water to form a solid film.[158] At the initial stage of water evaporation, the CNC suspension undergoes a phase transition into a biphasic stage of isotropic phase and cholesteric phase, then further transition into a pure cholesteric phase as described above. As the CNC concentration increases to ∼8 wt. %, the movement of CNCs becomes restricted, kinetic arrest occurs, and the helical structures are locked in place to form a gel.[35] Finally, a dried film with helical structures is formed upon complete evaporation of water, where the helical structures can be maintained, presumably because of the chirality transfer from molecular CNCs to the macroscopic LC order.[158] During this evaporation-induced self-assembly process, the helical pitch will be significantly reduced from micrometer-sized range to submicrometer-sized range.

It is crucial to control different parameters in the evaporation process to obtain desired and uniform pitch of the helical twists and structural colors in the final dried film. For example, an increase in ionic strength of the CNC suspension can decrease the helical pitch in the final film.[159] Relative humidity during evaporation,[160] the initial CNC concentration and polydispersity,[161] the evaporation rate,[162] and even the substrate surface chemistry[163] all play crucial roles in

TABLE II. Summary of different types of LCE composites.

	Materials	Incorporation method	Applications	References
Photothermal metallic nanoparticles	AuNP/LCE	Direct mixing	NA	63
	AuNS/LCE AuNR/LCE	Direct mixing	Photoresponsive actuator	77
	AuNP/LCE	Direct mixing	Photoresponsive actuator	99
	AuNR/LCE	Cross-link	Photoresponsive actuator	52
	AuNP/LCE	Cross-link	Photoresponsive actuator	50
	AuNR/LCE	Surface modification	Photoresponsive actuator	64, 146
	AuNP/LCE	*In situ* reduction	Photoresponsive actuator	101
Magnetic particles	Fe_4O_3/LCE	Cross-link	NA	105 and 106
	α-Fe_2O_3/LCE	Cross-link	Magnetic memory device	53
	γ-Fe_2O_3 NP/LCE	Cross-link	Photoresponsive actuator, transduction	147
	$BaFe_{12}O_{19}$/LCE	Cross-link	Magnetic responsive actuator	108
	Fe_3O_4/LCE	Surface modification	Magnetic responsive actuator	54, 55, and 111
	Fe_3O_4/LCE	Surface modification	Cell culture	109
	Co nanorod/LCE	Surface modification	Magnetic memory device	110
	NdFeB/LCE	Direct mixing	Magnetic responsive actuator	65 and 66
Liquid metal	LM/LCE	Direct mixing	Electrical actuator, sensor	56
		Direct mixing	Electrical, photoresponsive actuator	90
		Two phases	Electrical actuator, sensor	91,114,115, and 148
		Two phases	Thermal-responsive electrical switch	149
Carbon nanotubes	SWCNT/LCE	Direct mixing	Electrical actuator	121
	SWCNT/LCE	Direct mixing	Photoresponsive actuator	59 and 150
	CNT/LCE	Swell	NA	122, 123
	SWCNT/LCE	Surface modification	Photoresponsive actuator	57
	CNT/LCE	Surface modification	Photoresponsive actuator	125, 151–153
	SWCNT/LCE	Direct mixing	Photoresponsive actuator	126, 154, 155
	CNT/LCE	Direct mixing	Electrical actuator	67
	CNT/LCE	Direct mixing	Electrical, photoresponsive actuator	131
	CNT/LCE	Two phases	Electrical, photoresponsive actuator	68
	MWCNT/LCE	Direct mixing[a]	Photoresponsive actuator	156
Graphene and its derivatives	GO/LCE	Direct mixing	Photoresponsive actuator	138
	GO/LCE	Surface modification	Photoresponsive actuator	78
	rGO/LCE	Direct mixing	Photoresponsive actuator	139
Carbon black	CB/LCE	Direct mixing	Electrical actuator	140
		Swell	Electrical actuator	141
		Swell	Cell Culture	142
		Two phases	Electrical actuator	143
Other nanoparticles	$PbTiO_3$/LCE	Direct mixing	N.A.	144
	MoO_{3-x} /LCE	Direct mixing	N.A.	145

[a]Using polymer of intrinsically microporous as a dispersant.

controlling the CNC self-assembly process to obtain a uniform cholesteric phase and pitch. However, pure CNC films are very brittle, so the helical pitch in dried films is not tunable. It is important to improve the flexibility of the films while maintaining the helical structures. One promising approach is to form CNC/polymer composites with cholesteric LC ordering.

For example, PEG, a water-soluble polymer, is commonly used to co-assemble with CNCs to improve the flexibility and tune the helical pitch.[164–166] Bardet *et al.*[166] show that the film stretchability can be doubled by adding 10 wt. % PEG while maintaining the coloration in the composite film. However, when the PEG loading exceeds 30 wt. %, PEG and CNCs experience microphase separation, leading to disruption of the cholesteric LC order in CNCs.[165] In addition to increasing the flexibility, PEG can also improve the uniformity of helical pitches and structural coloration in the resulting films,[164] presumably due to the entropic depletion interactions between CNCs.[167,168] The separation distance between CNC rods is smaller than the radius of gyration of PEG, and PEG molecules are excluded from the regions around the

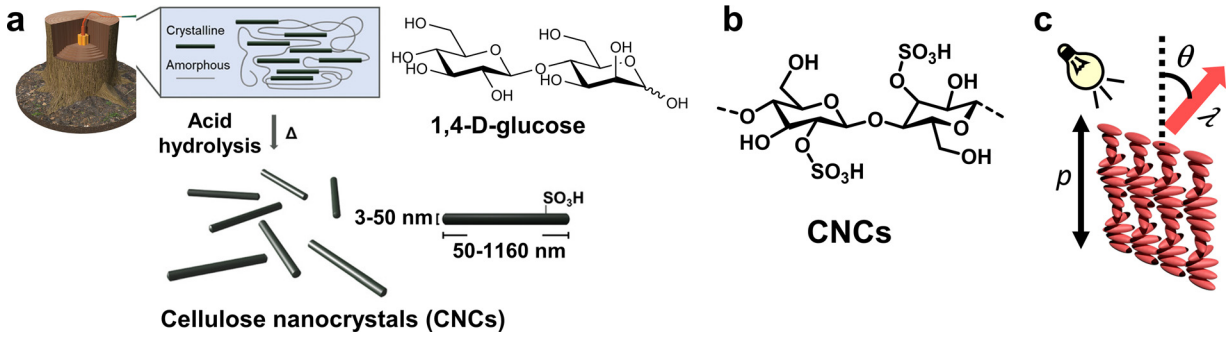

FIG. 10. CNCs and the helical superstructures. (a) Schematic illustration of CNC preparation from the wood.[2] Reproduced with permission from Tran *et al.*, Adv. Mater. **32,** 1905876 (2020). Copyright 2020 Wiley-VCH. (b) Chemical structure of CNCs. (c) Helical superstructures in CNCs and selective light reflection from CNCs.

CNC rods, so the osmotic pressure difference on two sides of each CNC rod will lead to an attractive force between CNC rods and facilitate the assembly of helical structures. Similarly, hydrophilic polymers glycerol[169] and polyethylene glycol diacrylate (PEGDA)[170] can be added in CNCs to improve film flexibility and achieve tunable structural colors.

External stimuli-responsive CNC/hydrogels can be formed by mixing CNCs with functional monomers such as temperature responsive N-isopropyl acrylamide (NIPAAm),[171] 2-hydroxyethylmethacrylate (HEMA), and pH responsive acrylic acid (AAc),[172] followed by evaporation-induced self-assembly and polymerization to lock the helical structures. Glutaraldehyde has been used as a bridging agent, which can react with hydroxyl groups from CNCs and amino groups from polyacrylamide (PAAm).[173]

In addition to direct mixing of CNCs with hydrogel precursors, Boott *et al.*[174] infiltrate hydrogel precursors after forming the dry CNC film, where glucose is used to promote uniform swelling and increase the swelling ratio. The glucose-CNC dry film is first treated with dimethyl sulfoxide (DMSO) and then infiltrated with hydrogel precursors, followed by cross-linking. The obtained film can be stretched up to 300%, changing color from red to blue.

To increase the compatibility between the aqueous CNC dispersion and other non-aqueous polymers, including poly(methyl methacrylate) (PMMA), polystyrene (PS), and polycarbonate (PC) to create photonic films, Cheung *et al.*[174] neutralize CNCs by strong bases, followed by freeze drying and redispersing in polar organic solvents such as DMSO and dimethylformamide (DMF) with a concentration ~3 wt. %. Further, CNCs can be surface functionalized by acetylation, desulfation, cationization, or tetramethylpiperidine (TEMPO)-oxidation,[175] allowing for *in situ* oxidative polymerization of pyrrole to form conductive CNC/polypyrrole composites.

CNC composites can also be achieved by freeze-casting to form anisotropic CNC aerogels first, followed by infiltration of poly(oligo ethylene glycol methacrylate) (POEGMA) and cross-linking.[176] The anisotropy of the CNC composite can be controlled by the ratio between CNC and POEGMA, freeze-casting temperature, and the concentrations of CNCs and POEGMA, resulting in various morphologies such as columnar, fibrillar, and lamellar. Liu *et al.*[177] report the fabrication of cellulose-based nematogels, where cellulose nanofibrils are first physically cross-linked by acid via hydrogen bonds between the carboxyl groups on cellulose nanofibrils, followed by an exchange with isopropanol and nematic LC small molecule 5CB.

IV. APPLICATIONS

A. Soft robotic actuators

Owing to the unique anisotropic deformation of LCEs during phase transition, they are widely used as soft robotic actuators to complete various tasks and work, yet their thermotropic responsiveness often results in slow actuation speed and low energy conversion efficiency due to the low heat dissipation efficiency. Therefore, LCE composites with different types of functional fillers are extensively studied to address these challenges over the past years.

AuNPs,[50,52,64,77] CNTs,[57,120,126] and GO[78] are often incorporated into LCEs to provide photothermal responsiveness to realize the remote and localized light actuation. For example, we show that AuNR/LCE composite films can be morphed into different shapes depending on the choices of photomasks.[64] The films can achieve fast actuation (response time ~5 s and a maximum actuation strain of 56%). Similarly, AuNPs are incorporated into LCEs to form composite fibers that can exhibit shrinkage under IR light exposure, acting as photoresponsive muscle-like robots.[50,52] When the cross-linked LCE is swelled by $HAuCl_4$ solution, which is selectively reduced to AuNPs by UV light using grayscale photomasks, the patterned AuNPs inside the LCE can lead to nonuniform photothermal heating and further programmable actuation upon IR light irradiation [Fig. 11(a)].[101]

Li *et al.*[126,155] show that the actuation of the LCE composite with SWCNTs can be triggered not only by IR light, but also by white light at an intensity of ~100 mW cm^{-2} for potential applications such as artificial heliotropism. The LCE composite is integrated with solar cells, with the composite actuator facing sunlight to contract and tilt the solar cell toward the sun. As a result, they observe a significant improvement in the output photocurrent of the solar cells. LCE/CNT composite filaments can function as artificial muscles for actuation. We fabricate meter-long LCE composite filaments as muscle-like actuators by extrusion, showing greatly improved mechanical property and IR light and electric field responsiveness.[120] The composite filament with 2 wt. % CNT loading can generate work within a certain period of time that is comparable to the value of mammal muscular skeleton systems, that is, possessing a maximum work capacity of 38 J/kg. They can be integrated into several soft robotic systems, including a swing set that can swing to either front or top and a hopping unicorn. Kohlmeyer *et al.*[58] design a bilayer gripper mimicking Venus flytrap from the CNT/LCE composite and silicone rubber. The open and close modes are controlled via IR light irradiation.

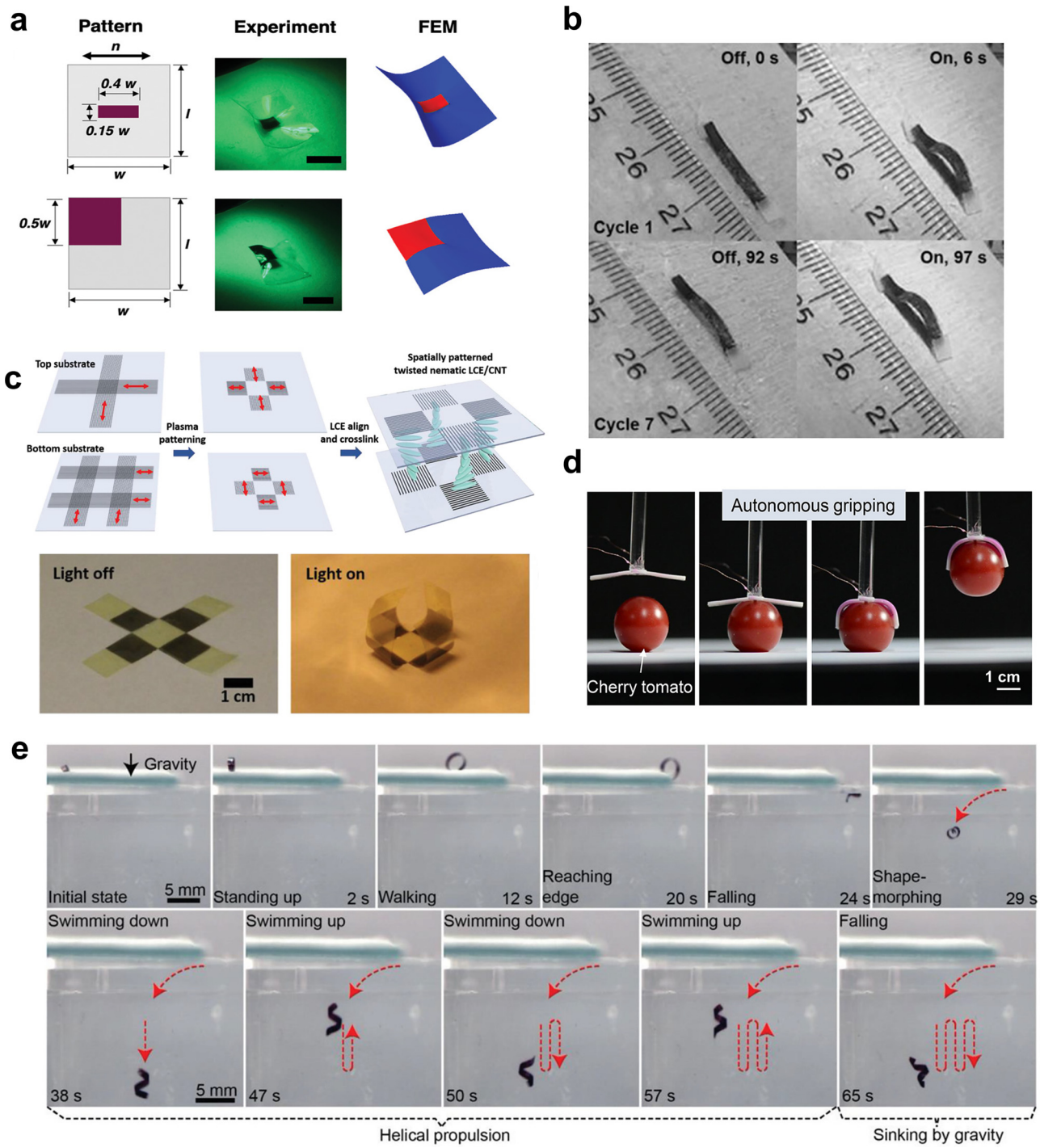

FIG. 11. LCE composites as soft robotic actuators. (a) Localized photothermal effect and shape transformation by patterning AuNPs.[101] Reproduced with permission from Kuenstler *et al.*, Adv. Mater. **32,** 2000609 (2020). Copyright 2020 Wiley-VCH. (b) Digital images of an inchworm walker made from CNT/LCE composite climbing on a tilted substrate.[58] Reproduced with permission from Kohlmeyer *et al.*, Angew. Chem. Int. Ed. **52**, 9234 (2013). Copyright 2013 Wiley-VCH. (c) Top: schematic illustration of plasma-patterning CNT sheets onto the LCE film. Bottom: localized photothermal origami actuation of the CNT/LCE composite film.[68] Reproduced with permission from Kim *et al.*, Adv. Funct. Mater. **29**, 1905063 (2019). Copyright 2019 Wiley-VCH. (d) Digital images of an artificial flytrap gripping a cherry tomato autonomously.[114] Reproduced with permission from Ma *et al.*, ACS Appl. Mater. Interfaces **13**, 5574 (2021). Copyright 2021 ACS. (e) Digital images of a soft miniature robot walking on a substrate and swimming in a viscous liquid.[65] Reproduced with permission from Zhang *et al.*, Adv. Mater. **33**, 2006191 (2021). Copyright 2021 Wiley-VCH.

An inchworm walker from the same composite film with polycarbonate caps at two ends to prevent sliding is also demonstrated [Fig. 11(b)]. The inchworm walker is capable of climbing on a tilted substrate with 50° slope at an average speed of 0.1 mm s^{-1}, where the moving direction of the walker is controlled by the direction of IR light. Compared to dispersing CNTs into the LCE matrix, Kim *et al.*[68] report the direct attachment of continuous CNT sheets on the LCE, where the twisted nematic LCE with a single layer CNT sheets on both sides can bend to a maximum angle of around 100° within 1.2 s and recover within 2.2 s under 287 mW cm^{-2} visible light. It also allows for actuation by the lamp of a cellular phone and unconcentrated sunlight. The location of CNT sheets can be controlled by oxygen plasma to program the photothermal heating magnitude in the film, such as realizing a folding actuator [Fig. 11(c)]. When the LCE matrix containing azobenzene moieties is used, together with the incorporation of the photothermal fillers, the composite films can realize both UV light and NIR light responsiveness.[154] Since most UV light is absorbed by the surface layer of the film, leading to shrinkage only on the surface, the overall film will bend toward the UV light. On the contrary, the irradiation of NIR light will heat the entire film and cause uniform shrinkage of the film. Moreover, photothermal fillers can be also utilized to improve the programming and reprogramming of LCEs when embedded into LCE with dynamic covalent bonds. Yang *et al.*[156] fabricate CNT/LCE composites with transesterification dynamic bonds, where the T_{NI} (120 °C) is lower than the reaction temperature of the dynamic bonds (160 °C). The resulting composites can not only be actuated by the NIR light, but also can be easily erased and reprogrammed to generate various structures without a mold when further heating to 160 °C by increasing the light power. As a result, a single six-petal "flower" can be reconfigured into more than 20 different actuation modes through light-induced transesterification.

In addition to the photothermal responsiveness, CNTs[67,68] and LM[56,91,114,115] are introduced to endow LCE composites with electrical responsiveness. Guin *et al.*[67] report the electrical actuation of the LCE composite film with 0.02 wt. % SWCNTs. They observe 18% contraction of the composite film at 100 °C within 1 s at 5 V/μm as well as a rapid recovery in less than 1 s after removing the electric field. They claim that the deformation is not caused by the electrothermal effect; since the film is only heated by 3 °C in 60 s, rather, this electromechanical response can be attributed to the SWCNT rotation arising from the dielectric mismatch between the LCE matrix and SWCNTs. When the CNT/LCE composite film with CNT sheets attached to the LCE is twisted into a fiber, it exhibits a maximum work capacity of 97 kJ m^{-3} by a DC voltage of 15.1 V cm^{-2} through the Joule heating.[68]

Taking advantage of the high conductivity, intrinsic soft nature of the LM, Ambulo *et al.*[90] 3D print LCE composite containing of 88 wt. % LM, where LM droplets are percolated with resistivity ranging from 0.0038 to 0.035 Ω cm. The resulting LM/LCE shows reversible actuation strain of ∼12% by an 8.9 W cm^{-3} electrical power. The actuation strain is much smaller compared to that without LM inclusion, ∼45%, which could be due to insufficient cross-linking during 3D printing arising from LM inhibition and decrease in the nematic order. Similarly, Ford *et al.*[56] fabricate the LCE composite film with 83 wt. % LM that becomes electrically conductive after mechanical sintering, serving as a transducer to sense finger touch, an electrothermally responsive actuator for weightlifting, and a conductive pathway for lightening an LED. Sun *et al.*[148] have also fabricated LM/LCE fibers with large contraction ratios and electrical responsiveness, where the contraction ratio and rate can be programmed by adjusting voltage and pulse time. The fibers can produce over 40% contraction ratio at a rate of 280% s^{-1} under 1.25 V cm^{-1}. They further use the fibers to mimic human triceps muscle for ball shooting. Kotikian *et al.*[91] design innervated LCE actuators with the LM core and the LCE shell that can self-sense and realize closed-loop control even with large bias weights. Because the resistance is closely related to the contractile strain and temperature during Joule heating, they set a target normalized resistance (R/R_0), which can automatically regulate the resistance feedback of the innervated LCE actuator, where the actuator can track self-sensing actuation while omitting perturbation up to 4.2 grams in 20 s. Based on the similar mechanism, Ma *et al.*[114] realize an artificial fly-trap that can autonomously grip an object by sensing the contact pressure and redistributing the current in the conductive loop. The gripper can grab a cherry tomato with a weight of 7.2 g that is ten times larger than the mass of the gripper itself [Fig. 11(d)].

Although the magnetic particles also exhibit a magnetic heating effect that can be used to trigger the phase transition of LCE,[54] the magnetic field responsiveness is more attractive, as it provides an additional degree of freedom to control the composite actuator independently and wirelessly, which is especially beneficial for soft miniature robots. Ditter *et al.*[111] fabricate Fe_3O_4/LCE composite microparticles, which can be guided by an external magnetic field to move and transport goods including textiles, plastic, and copper. Zhang *et al.*[65] embed magnetic microparticles inside the LCE containing azobenzene moieties to realize multi-responsiveness. For example, the soft robot can walk forward on the substrate by controlling the external magnetic field. After the soft robot falls into a 70 °C liquid, the shape morphing behavior is triggered to transfer the robot into a helical structure according to the preprogrammed LC director field, while the robot is manipulated to rotate in the liquid controlled by the rotatory magnetic field [Fig. 11(e)]. Similarly, Li *et al.*[66] design a biomimetic "bug" robot from magnetic particle/LCE composites that can jump, roll across an obstacle, and pass through a crack activated by either a magnetic field or temperature variation.

B. Photonic displays

Compared to pigment colors, structural colors are environmentally more stable since they are generated from reflection, diffraction, and scattering of interference light from photonic crystals consisting of quasi-amorphous structures or periodic structures.[178] For example, cholesteric LCs with helical pitch in the visible wavelength are of great interest for photonic displays. In CNC hydrogel composites, CNCs with helical superstructures provide photonic crystal properties, whereas the water absorption nature of hydrogels introduces humidity responsiveness to the composites.

Lu *et al.*[173] design a stable photonic humidity sensor by covalently bonding PAAm with CNCs, where humidity change is indicated by the swelling ratio of PAAm hydrogel and thus shift of the structure color of the composite color, for example, from green to red as relative humidity increased from 11% to 97%, corresponding to a wavelength change of 92 nm. Yao *et al.*[164] co-assemble CNCs with PEG under slow drying conditions [Fig. 12(a)]. The resulting film shows uniform helical pitches with a reversible structural color transformation between transparent and green when the humidity changes between 100% and 50%, which is attributed to the swelling and deswelling of

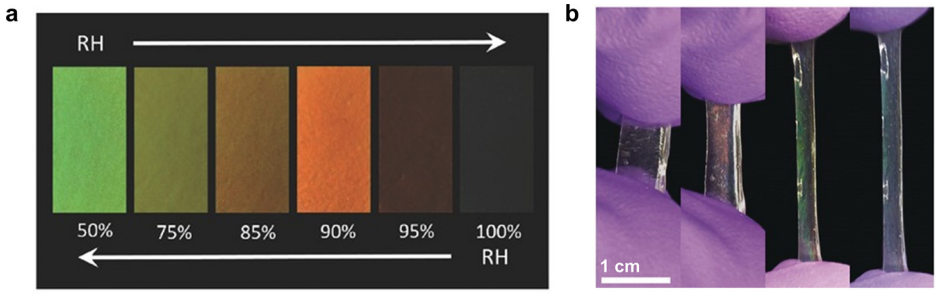

FIG. 12. Tunable structural colors in CNC composites as photonic devices. (a) Digital images showing structural color variation in a CNC/PEG composite film in response to relative humidity change.[164] Reproduced with permission from Yao *et al.*, Adv. Mater. **29,** 1701323 (2017). Copyright 2017 Wiley-VCH. (b) Digital image showing a blue shift of color in a CNC elastomer film by stretching up to 300%.[179] Reproduced with permission from Boott *et al.*, Angew. Chem. Int. Ed. **59,** 226 (2020). Copyright 2020 Wiley-VCH.

the film. Similarly, glycerol,[169] polyethylene glycol diacrylate (PEGDA),[170] and AAc[172] are also added in CNCs to realize the structural color change in response to the humidity change.

Boott *et al.*[179] integrate CNCs with ethyl acrylate and 2-hydroxyethyl acrylate hydrogels to realize a stretchable CNC elastomer with a maximum strain of 300%. During the mechanical stretching process, the structural color shifts from red to blue [Fig. 12(b)] due to the helical pitch compression. Although the mechanical stress causes unwinding of chiral twist into small domains of pseudo-nematic structures, the overall helical structures are preserved to exhibit structural color. In addition, Chen *et al.*[180] introduce boronic esters as the dynamic covalent bond such that the resulting CNC/PVA-PAAm composite hydrogels exhibit self-healing property.

C. Cell culture and tissue engineering

LCEs with reversible and anisotropic shape deformation are beneficial for biomedical applications such as tissue engineering and cell culture. By programming the molecular orientation of LC mesogens inside LCEs, cell alignment can be potentially guided and oriented along the LC alignment direction. Instead of controlling cellular behavior on LCE surfaces by heat, the introduction of nanoparticles allows for remote control of cell culture.

For example, Herrera-Posada *et al.*[109] fabricate Fe_3O_4/LCE nanocomposite films, where the mechanical deformation can be remotely manipulated by a magnetic field based on heat generation from iron oxide. To improve the biocompatibility of Fe_3O_4/LCE nanocomposite with cells, the nanocomposite is surface treated with collagen and the resulting film can attach and proliferate NIH-3T3 fibroblasts. Fe_3O_4/LCE nanocomposite films with tunable deformation offer a platform for studying the effect of dynamic mechanical properties on fibroblast cell culture. Similarly, Agrawal *et al.*[142] introduce CB nanoparticles to trigger electromechanical deformation of the LCE composite based on Joule heating effect. After surface functionalized with collagen to improve cell attachment, the CB/LCE composite film, which exhibits a maximum contraction of up to 30% with a response time of 0.6 s over 5000 cycles, is used for dynamic cell culture of neonatal rat ventricular myocytes (NRVM). Due to faster heat dissipation in the water environment and thus lower film surface temperature during LCE phase transition, NRVM remains viable when the electromechanical response of the LCE composite is triggered. Although the unique property of molecular anisotropy in LCE composites is promising for studying dynamic cell culture, issues such as cell adhesion and viability on LCE composites need to be addressed in the future.

D. Other applications

Tactile sensors with realistic haptic feedback play an important role in the development of virtual reality technologies,[181] where LCE composites with controllable actuation and multi-responsiveness are beneficial. For instance, Camargo *et al.*[151,152] design a light-responsive tactile device from the CNT/LCE composite. They couple thermal cross-linking with mechanical stretching during the molding process to obtain monodomain LC mesogens along the side walls in the mold. As a result, the "bubble-like" patterns can contract upon light irradiation with 10.22% shrinkage. The integration of LM and magnetic particles adds additional functionality and responsiveness, potentially providing locally controllable haptic sensing.

Magnetic particles can also be used to store anisotropic information in LCEs. For example, Haberl *et al.*[147] introduce anisotropic γ-Fe_2O_3 nanospindles in LCEs with both magnetic and optical responses. Owing to the high absorption coefficient of γ-Fe_2O_3 nanospindles at 532 nm, the LCE composite can be deformed by green light irradiation. The γ-Fe_2O_3 nanospindles inside the composite exhibit continuous reorientation during the light-triggered actuation, which can be monitored by a vibrating sample magnetometer, so that the light signal is converted into magnetic readout and potentially used as transducers.

V. CONCLUDING REMARKS AND OUTLOOK

In this review, we overview recent advances in LCE composites from a broad perspective, where LCE composites are defined as elastomeric composites with embedded liquid crystallinity from either thermotropic or lyotropic LC phases. Due to their embedded anisotropy, the responsiveness can be manipulated over multiple length scales with programmability, efficiency, and spatially adaptable controllability. For LCE composites made from thermotropic LCEs with fillers including metallic nanoparticles, magnetic particles, LM, CNTs, graphene derivatives, and CB, the coupling between the functionality of fillers and the anisotropic shape deformation from LCEs leads to improved mechanical, thermal, optical, and electrical properties. The interaction between fillers and the LCE matrix, strategies to improve their compatibility via chemical synthesis and surface modification, have been thoroughly discussed. Meanwhile, LCE composites from lyotropic LC phases

such as CNC hydrogels can form helical twists, often with photonic crystal structures and structural color. Methods to integrate CNC self-assembly with hydrogels have been overviewed, with an emphasis on the tunability of helical structures and structural color. Finally, various applications of LCE composites including soft robotics, photonic displays, tissue engineering, and other applications are highlighted.

Currently, the design of the LCE composite is mainly considered from the aspects of enhancing or endows extra properties and functionalities of the LCE by embedding fillers. However, can the LCE also benefit the fillers we choose, especially when the fillers are also anisotropic? For example, we have seen the CNTs and AuNRs can be aligned with the LCE director, where the anisotropy can be coupled in their mechanical performance. Whether the aligned fillers in the LCE can offer composites with unique nonlinear optical, acoustical properties, or increase the energy conversion efficiency during the reversible actuation? Meanwhile, it is challenging to increase the loading of the fillers into LCEs without significant aggregation. For example, CNTs and graphene are highly conductive materials. However, even at the highest loading amount reported (3 wt. % for CNTs,[125] less than 1 wt. % for graphene[138]) the composites are not electrically conductive due to poor dispersity, whereas high conductivity is important for soft robotics and soft electronics. The alignment control is the key parameter to be considered for LCE composite applications. With the fast development of 3D printing techniques, LCE composites can be designed to realize 3D shape transformation within micrometer-scaled resolution via 3D printing, where the material properties and responsiveness are tunable depending on the choice of fillers. Despite recent progress, the printed structures are often limited to relatively simple geometry such as cones, ribbons, and grids without fully utilizing the functions of the fillers. By considering the relationship between chemistry, structure, and functionality, LCE composites offer opportunities to embed both chemical and physical intelligence with extra degrees of controllability via geometries. In turn, it will offer new insights to engineer the next-generation multi-functional materials with unique acoustical, optical, mechanical, and electrical properties for potential applications such as flexible circuitry[182] that can change shape and electrical conductivity by harvesting environmental resources, smart wearables,[183] tunable and packable antenna,[184] and camouflage and displays.[185] It will also be intriguing to create biocompatible and sustainable LCE composites from abundant natural biomass materials such as cellulose nanocrystals[2] and silk fibers.[186]

ACKNOWLEDGMENTS

The authors acknowledge financial support from National Science Foundation (NSF) through the University of Pennsylvania Materials Research Science and Engineering Center (MRSEC), No. DMR-1720530, DMR/Polymer program, No. DMR-210484, and Future Eco Manufacturing Research Grant (FMRG), No. CMMI 2037097.

AUTHOR DECLARATIONS

Conflict of Interest

The authors have no conflicts to disclose.

Author Contributions

Y.W. and J.L. contributed equally to this work.

DATA AVAILABILITY

Data sharing is not applicable to this article as no new data were created or analyzed in this study.

REFERENCES

[1]T. Geelhaar, K. Griesar, and B. Reckmann, Angew. Chem. Int. Ed. **52**, 8798 (2013).
[2]A. Tran, C. E. Boott, and M. J. MacLachlan, Adv. Mater. **32**, 1905876 (2020).
[3]T. C. Lubensky, D. Pettey, N. Currier, and H. Stark, Phys. Rev. E **57**, 610 (1998).
[4]L. Wang, A. M. Urbas, and Q. Li, Adv. Mater. **32**, 1801335 (2020).
[5]L. Onsager, Ann. N. Y. Acad. Sci. **51**, 627 (1949).
[6]I. Dierking and S. Al-Zangana, Nanomaterials **7**, 305 (2017).
[7]R. Narayan, J. E. Kim, J. Y. Kim, K. E. Lee, and S. O. Kim, Adv. Mater. **28**, 3045 (2016).
[8]Y. Xia, T. S. Mathis, M.-Q. Zhao, B. Anasori, A. Dang, Z. Zhou, H. Cho, Y. Gogotsi, and S. Yang, Nature **557**, 409 (2018).
[9]K. Steck, S. Dieterich, C. Stubenrauch, and F. Giesselmann, J. Mater. Chem. C **8**, 5335 (2020).
[10]H.-S. Park, S.-W. Kang, L. Tortora, Y. Nastishin, D. Finotello, S. Kumar, and O. D. Lavrentovich, J. Phys. Chem. B **112**, 16307 (2008).
[11]M. Camacho-Lopez, H. Finkelmann, P. Palffy-Muhoray, and M. Shelley, Nat. Mater. **3**, 307 (2004).
[12]S. V. Ahir, A. R. Tajbakhsh, and E. M. Terentjev, Adv. Funct. Mater. **16**, 556 (2006).
[13]T. H. Ware, J. S. Biggins, A. F. Shick, M. Warner, and T. J. White, Nat. Commun. **7**, 10781 (2016).
[14]P. G. De Gennes, Phys. Lett. **28**, 725 (1969).
[15]T. J. White and D. J. Broer, Nat. Mater. **14**, 1087 (2015).
[16]O. M. Wani, H. Zeng, and A. Priimagi, Nat. Commun. **8**, 15546 (2017).
[17]S. Iamsaard, S. J. Asshoff, B. Matt, T. Kudernac, J. J. Cornelissen, S. P. Fletcher, and N. Katsonis, Nat. Chem. **6**, 229 (2014).
[18]M. Wang, B. P. Lin, and H. Yang, Nat. Commun. **7**, 13981 (2016).
[19]T. H. Ware, M. E. McConney, J. J. Wie, V. P. Tondiglia, and T. J. White, Science **347**, 982 (2015).
[20]M. Warner, P. Bladon, and E. Terentjev, J. Phys. II **4**, 93 (1994).
[21]E. M. Terentjev, J. Phys. Condens. Matter **11**, R239 (1999).
[22]J. S. Biggins, M. Warner, and K. Bhattacharya, Phys. Rev. Lett. **103**, 037802 (2009).
[23]A. D. Auguste, J. W. Ward, J. O. Hardin, B. A. Kowalski, T. C. Guin, J. D. Berrigan, and T. J. White, Adv. Mater. **30**, 1802438 (2018).
[24]J. Küpfer and H. Finkelmann, Makromol. Chem. Rapid Commun. **12**, 717 (1991).
[25]H. Finkelmann, H.-J. Kock, and G. Rehage, Makromol. Chem. Rapid Commun. **2**, 317 (1981).
[26]G. H. F. Bergmann, H. Finkelmann, V. Percec, and M. Zhao, Macromol. Rapid. Commun. **18**, 353 (1997).
[27]B. Donnio, H. Wermter, and H. Finkelmann, Macromolecules **33**, 7724 (2000).
[28]N. Torras, K. E. Zinoviev, J. Esteve, and A. Sánchez-Ferrer, J. Mater. Chem. C **1**, 5183 (2013).
[29]T. H. Ware, Z. P. Perry, C. M. Middleton, S. T. Iacono, and T. J. White, ACS Macro Lett. **4**, 942 (2015).
[30]C. M. Yakacki, M. Saed, D. P. Nair, T. Gong, S. M. Reed, and C. N. Bowman, RSC Adv. **5**, 18997 (2015).
[31]Y. Xia, X. Zhang, and S. Yang, Angew. Chem. Int. Ed. **57**, 5665 (2018).
[32]T. H. Ware and T. J. White, Polym. Chem. **6**, 4835 (2015).
[33]M. O. Saed, R. H. Volpe, N. A. Traugutt, R. Visvanathan, N. A. Clark, and C. M. Yakacki, Soft Matter **13**, 7537 (2017).
[34]N. P. Godman, B. A. Kowalski, A. D. Auguste, H. Koerner, and T. J. White, ACS Macro Lett. **6**, 1290 (2017).
[35]J. M. McCracken, B. R. Donovan, K. M. Lynch, and T. J. White, Adv. Funct. Mater. **31**, 2100564 (2021).
[36]M. T. Brannum, A. M. Steele, M. C. Venetos, L. T. J. Korley, G. E. Wnek, and T. J. White, Adv. Opt. Mater. **7**, 1801683 (2019).

[37]Z. Pei, Y. Yang, Q. Chen, E. M. Terentjev, Y. Wei, and Y. Ji, Nat. Mater. **13**, 36 (2014).
[38]M. O. Saed, A. Gablier, and E. M. Terentejv, Adv. Funct. Mater. **30**, 1906458 (2020).
[39]Z. Wen, M. K. McBride, X. Zhang, X. Han, A. M. Martinez, R. Shao, C. Zhu, R. Visvanathan, N. A. Clark, Y. Wang, K. Yang, and C. N. Bowman, Macromolecules **51**, 5812 (2018).
[40]M. K. McBride, M. Hendrikx, D. Liu, B. T. Worrell, D. J. Broer, and C. N. Bowman, Adv. Mater. **29**, 1606509 (2017).
[41]Z. Wang, H. Tian, Q. He, and S. Cai, ACS Appl. Mater. Interfaces **9**, 33119 (2017).
[42]S. W. Ula, N. A. Traugutt, R. H. Volpe, R. R. Patel, K. Yu, and C. M. Yakacki, Liq. Cryst. Rev. **6**, 78 (2018).
[43]R. S. Kularatne, H. Kim, J. M. Boothby, and T. H. Ware, J. Polym. Sci. B **55**, 395 (2017).
[44]D. Martella and C. Parmeggiani, Chem. Eur. J. **24**, 12206 (2018).
[45]Z. Wang and S. Cai, J. Mater. Chem. B **8**, 6610 (2020).
[46]M. O. Saed, A. Gablier, and E. M. Terentjev, Chem. Rev. (to be published 2021).
[47]C. Ohm, M. Brehmer, and R. Zentel, Adv. Mater. **22**, 3366 (2010).
[48]K. M. Herbert, H. E. Fowler, J. M. McCracken, K. R. Schlafmann, J. A. Koch, and T. J. White, Nat. Rev. Mater. (to be published 2021).
[49]M. Barnes and R. Verduzco, Soft Matter **15**, 870 (2019).
[50]J. Xu, S. Chen, W. Yang, B. Qin, X. Wang, Y. Wang, M. Cao, Y. Gao, C. Li, and Y. Dong, Soft Matter **15**, 6116 (2019).
[51]M. M. Wójcik, J. Wróbel, Z. Z. Jańczuk, J. Mieczkowski, E. Górecka, J. Choi, M. Cho, and D. Pociecha, Chem. Eur. J. **23**, 8912 (2017).
[52]H. Yang, J. J. Liu, Z. F. Wang, L. X. Guo, P. Keller, B. P. Lin, Y. Sun, and X. Q. Zhang, Chem. Commun. **51**, 12126 (2015).
[53]J. M. Haberl, A. Sanchez-Ferrer, A. M. Mihut, H. Dietsch, A. M. Hirt, and R. Mezzenga, Adv. Mater. **25**, 1787 (2013).
[54]M. Winkler, A. Kaiser, S. Krause, H. Finkelmann, and A. M. Schmidt, Macromol. Symp. **291–292**, 186 (2010).
[55]A. Kaiser, M. Winkler, S. Krause, H. Finkelmann, and A. M. Schmidt, J. Mater. Chem. **19**, 538 (2009).
[56]M. J. Ford, C. P. Ambulo, T. A. Kent, E. J. Markvicka, C. Pan, J. Malen, T. H. Ware, and C. Majidi, Proc. Natl. Acad. Sci. U. S. A. **116**, 21438 (2019).
[57]L. Yang, K. Setyowati, A. Li, S. Gong, and J. Chen, Adv. Mater. **20**, 2271 (2008).
[58]R. R. Kohlmeyer and J. Chen, Angew. Chem. Int. Ed. **52**, 9234 (2013).
[59]S. Ahir, A. Squires, A. Tajbakhsh, and E. Terentjev, Phys. Rev. B **73**, 085420 (2006).
[60]S. Kumar, J.-H. Kim, and Y. Shi, Phys. Rev. Lett. **94**, 077803 (2005).
[61]F. Weigert, Sci. Nat. **9**, 583 (1921).
[62]H. Aharoni, Y. Xia, X. Zhang, R. D. Kamien, and S. Yang, Proc. Natl. Acad. Sci. U. S. A. **115**, 7206 (2018).
[63]R. Montazami, C. M. Spillmann, J. Naciri, and B. R. Ratna, Sens. Actuators, B **178**, 175 (2012).
[64]Y. Wang, A. Dang, Z. Zhang, R. Yin, Y. Gao, L. Feng, and S. Yang, Adv. Mater. **32**, 2004270 (2020).
[65]J. Zhang, Y. Guo, W. Hu, R. H. Soon, Z. S. Davidson, and M. Sitti, Adv. Mater. **33**, 2006191 (2021).
[66]Y. Li, H. Yu, K. Yu, X. Guo, and X. Wang, Adv. Funct. Mater. **31**, 2100338 (2021).
[67]T. Guin, B. A. Kowalski, R. Rao, A. D. Auguste, C. A. Grabowski, P. F. Lloyd, V. P. Tondiglia, B. Maruyama, R. A. Vaia, and T. J. White, ACS Appl. Mater. Interfaces **10**, 1187 (2018).
[68]H. Kim, J. A. Lee, C. P. Ambulo, H. B. Lee, S. H. Kim, V. V. Naik, C. S. Haines, A. E. Aliev, R. Ovalle-Robles, R. H. Baughman, and T. H. Ware, Adv. Funct. Mater. **29**, 1905063 (2019).
[69]B. A. Kowalski, V. P. Tondiglia, T. Guin, and T. J. White, Soft Matter **13**, 4335 (2017).
[70]R.-Q. Ma and D.-K. Yang, Phys. Rev. E **61**, 1567 (2000).
[71]P. A. Kossyrev, J. Qi, N. V. Priezjev, R. A. Pelcovits, and G. P. Crawford, Appl. Phys. Lett. **81**, 2986 (2002).
[72]D. Liu, C. W. M. Bastiaansen, J. M. J. den Toonder, and D. J. Broer, Angew. Chem. Int. Ed. **51**, 892 (2012).
[73]S.-J. Ge, T.-P. Zhao, M. Wang, L.-L. Deng, B.-P. Lin, X.-Q. Zhang, Y. Sun, H. Yang, and E.-Q. Chen, Soft Matter **13**, 5463 (2017).
[74]H. Yang, A. Buguin, J.-M. Taulemesse, K. Kaneko, S. Méry, A. Bergeret, and P. Keller, J. Am. Chem. Soc. **131**, 15000 (2009).
[75]A. Buguin, M.-H. Li, P. Silberzan, B. Ladoux, and P. Keller, J. Am. Chem. Soc. **128**, 1088 (2006).
[76]Y. Yao, J. T. Waters, A. V. Shneidman, J. Cui, X. Wang, N. K. Mandsberg, S. Li, A. C. Balazs, and J. Aizenberg, Proc. Natl. Acad. Sci. U. S. A. **115**, 12950 (2018).
[77]X. Liu, R. Wei, P. T. Hoang, X. Wang, T. Liu, and P. Keller, Adv. Funct. Mater. **25**, 3022 (2015).
[78]R. Wei, Z. Wang, H. Zhang, and X. Liu, Liq. Cryst. **43**, 1009 (2016).
[79]R. L. Truby and J. A. Lewis, Nature **540**, 371 (2016).
[80]S. Li, H. Bai, Z. Liu, X. Zhang, C. Huang, L. W. Wiesner, M. Silberstein, and R. F. Shepherd, Sci. Adv. **7**, eabg3677 (2021).
[81]J. A. Lewis, Adv. Funct. Mater. **16**, 2193 (2006).
[82]M. K. Hausmann, P. A. Ruhs, G. Siqueira, J. R. Läuger, R. Libanori, T. Zimmermann, and A. R. Studart, ACS Nano **12**, 6926 (2018).
[83]A. Kotikian, R. L. Truby, J. W. Boley, T. J. White, and J. A. Lewis, Adv. Mater. **30**, 1706164 (2018).
[84]M. Lopez-Valdeolivas, D. Liu, D. J. Broer, and C. Sanchez-Somolinos, Macromol. Rapid. Commun. **39**, 1700710 (2018).
[85]C. P. Ambulo, J. J. Burroughs, J. M. Boothby, H. Kim, M. R. Shankar, and T. H. Ware, ACS Appl. Mater. Interfaces **9**, 37332 (2017).
[86]M. O. Saed, C. P. Ambulo, H. Kim, R. De, V. Raval, K. Searles, D. A. Siddiqui, J. M. O. Cue, M. C. Stefan, M. R. Shankar, and T. H. Ware, Adv. Funct. Mater. **29**, 1806412 (2019).
[87]A. Kotikian, C. McMahan, E. C. Davidson, J. M. Muhammad, R. D. Weeks, C. Daraio, and J. A. Lewis, Sci. Rob. **4**, eaax7044 (2019).
[88]C. Zhang, X. Lu, G. Fei, Z. Wang, H. Xia, and Y. Zhao, ACS Appl. Mater. Interfaces **11**, 44774 (2019).
[89]Z. Wang, Z. Wang, Y. Zheng, Q. He, Y. Wang, and S. Cai, Sci. Adv. **6**, eabc0034 (2020).
[90]C. P. Ambulo, M. J. Ford, K. Searles, C. Majidi, and T. H. Ware, ACS Appl. Mater. Interfaces **13**, 12805 (2021).
[91]A. Kotikian, J. M. Morales, A. Lu, J. Mueller, Z. S. Davidson, J. W. Boley, and J. A. Lewis, Adv. Mater. **33**, 2101814 (2021).
[92]S. Schuhladen, F. Preller, R. Rix, S. Petsch, R. Zentel, and H. Zappe, Adv. Mater. **26**, 7247 (2014).
[93]Z. L. Wu, A. Buguin, H. Yang, J.-M. Taulemesse, N. L. Moigne, A. Bergeret, X. Wang, and P. Keller, Adv. Funct. Mater. **23**, 3070 (2013).
[94]J. T. Waters, S. Li, Y. Yao, M. M. Lerch, M. Aizenberg, J. Aizenberg, and A. C. Balazs, Sci. Adv. **6**, eaay5349 (2020).
[95]M. Tabrizi, T. H. Ware, and M. R. Shankar, ACS Appl. Mater. Interfaces **11**, 28236 (2019).
[96]Y. Liu, B. Xu, S. Sun, J. Wei, L. Wu, and Y. Yu, Adv. Mater. **29**, 1604792 (2017).
[97]T. Guin, M. J. Settle, B. A. Kowalski, A. D. Auguste, R. V. Beblo, G. W. Reich, and T. J. White, Nat. Commun. **9**, 2531 (2018).
[98]Y. Xia, G. Cedillo-Servin, R. D. Kamien, and S. Yang, Adv. Mater. **28**, 9637 (2016).
[99]Y. Sun, J. S. Evans, T. Lee, B. Senyuk, P. Keller, S. He, and I. I. Smalyukh, Appl. Phys. Lett. **100**, 241901 (2012).
[100]Y. Xue, X. Li, H. Li, and W. Zhang, Nat. Commun. **5**, 4348 (2014).
[101]A. S. Kuenstler, Y. Chen, P. Bui, H. Kim, A. DeSimone, L. Jin, and R. C. Hayward, Adv. Mater. **32**, 2000609 (2020).
[102]Y. Shi, C. Zhu, J. Li, J. Wei, and J. Guo, New J. Chem. **40**, 7311 (2016).
[103]M. Bi, Y. Shao, Y. Wang, J. Zhang, H. Niu, Y. Gao, B. Wang, and C. Li, Mol. Cryst. Liq. Cryst. **652**, 41 (2017).
[104]W. F. Brown, Jr., J. Appl. Phys. **30**, S130 (1959).
[105]H. M. Song, J. C. Kim, J. H. Hong, Y. B. Lee, J. Choi, J. I. Lee, W. S. Kim, J. H. Kim, and N. H. Hur, Adv. Funct. Mater. **17**, 2070 (2007).
[106]A. Garcia-Márquez, A. Demortière, B. Heinrich, D. Guillon, S. Bégin-Colin, and B. Donnio, J. Mater. Chem. **21**, 8994 (2011).
[107]J. M. Haberl, A. Sanchez-Ferrer, A. M. Mihut, H. Dietsch, A. M. Hirt, and R. Mezzenga, Nanoscale **5**, 5539 (2013).
[108]L. Cmok, M. Vilfan, S. Gyergyek, and M. Čopič, Liq. Cryst. **2021**, 1.
[109]S. Herrera-Posada, C. Mora-Navarro, P. Ortiz-Bermudez, M. Torres-Lugo, K. M. McElhinny, P. G. Evans, B. O. Calcagno, and A. Acevedo, Mater. Sci. Eng. C **65**, 369 (2016).

[110]O. Riou, B. Lonetti, R. P. Tan, J. Harmel, K. Soulantica, P. Davidson, A. F. Mingotaud, M. Respaud, B. Chaudret, and M. Mauzac, Angew. Chem. Int. Ed. **54**, 10811 (2015).
[111]D. Ditter, P. Blümler, B. Klöckner, J. Hilgert, and R. Zentel, Adv. Funct. Mater. **29**, 1902454 (2019).
[112]T. V. Neumann and M. D. Dickey, Adv. Mater. Technol. **5**, 2000070 (2020).
[113]M. J. Ford, M. Palaniswamy, C. P. Ambulo, T. H. Ware, and C. Majidi, Soft Matter **16**, 5878 (2020).
[114]B. Ma, C. Xu, L. Cui, C. Zhao, and H. Liu, ACS Appl. Mater. Interfaces **13**, 5574 (2021).
[115]T. A. Kent, M. J. Ford, E. J. Markvicka, and C. Majidi, Multifunct. Mater. **3**, 025003 (2020).
[116]H.-C. Wu, X. Chang, L. Liu, F. Zhao, and Y. Zhao, J. Mater. Chem. **20**, 1036 (2010).
[117]B. Kumanek and D. Janas, J. Mater. Sci. **54**, 7397 (2019).
[118]K.-T. Lau, C. Gu, and D. Hui, Composites B **37**, 425 (2006).
[119]N. Karousis, N. Tagmatarchis, and D. Tasis, Chem. Rev. **110**, 5366 (2010).
[120]J. Liu, Y. Gao, H. Wang, R. Poling-Skutvik, C. O. Osuji, and S. Yang, Adv. Intell. Syst. **2**, 1900163 (2020).
[121]S. Courty, J. Mine, A. Tajbakhsh, and E. Terentjev, Europhys. Lett. **64**, 654 (2003).
[122]M. Chambers, B. Zalar, M. Remškar, J. Kovač, H. Finkelmann, and S. Žumer, Nanotechnology **18**, 415706 (2007).
[123]M. Chambers, B. Zalar, M. Remskar, H. Finkelmann, and S. Zumer, Nanotechnology **19**, 155501 (2008).
[124]J. Chen, H. Liu, W. A. Weimer, M. D. Halls, D. H. Waldeck, and G. C. Walker, J. Am. Chem. Soc. **124**, 9034 (2002).
[125]Y. Ji, Y. Y. Huang, R. Rungsawang, and E. M. Terentjev, Adv. Mater. **22**, 3436 (2010).
[126]C. Li, Y. Liu, C.-W. Lo, and H. Jiang, Soft Matter **7**, 7511 (2011).
[127]H. Koerner, G. Price, N. A. Pearce, M. Alexander, and R. A. Vaia, Nat. Mater. **3**, 115 (2004).
[128]S. V. Ahir and E. M. Terentjev, Nat. Mater. **4**, 491 (2005).
[129]R. A. Mrozek and T. A. Taton, Chem. Mater. **17**, 3384 (2005).
[130]I. Dierking, G. Scalia, and P. Morales, J. Appl. Phys. **97**, 044309 (2005).
[131]T. Guin, H. E. Hinton, E. Burgeson, C. C. Bowland, L. T. Kearney, Y. Li, I. Ivanov, N. A. Nguyen, and A. K. Naskar, Adv. Intell. Syst. **2**, 2000022 (2020).
[132]W. Bauhofer and J. Z. Kovacs, Compos. Sci. Technol. **69**, 1486 (2009).
[133]C. Lee, X. Wei, J. W. Kysar, and J. Hone, Science **321**, 385 (2008).
[134]A. A. Balandin, S. Ghosh, W. Bao, I. Calizo, D. Teweldebrhan, F. Miao, and C. N. Lau, Nano Lett. **8**, 902 (2008).
[135]S. Morozov, K. Novoselov, M. Katsnelson, F. Schedin, D. Elias, J. A. Jaszczak, and A. Geim, Phys. Rev. Lett. **100**, 016602 (2008).
[136]D. de Melo-Diogo, R. Lima-Sousa, C. G. Alves, and I. J. J. B. S. Correia, Biomater. Sci. **7**, 3534 (2019).
[137]O. C. Compton and S. T. Nguyen, Small **6**, 711 (2010).
[138]C. Li, Y. Liu, X. Huang, C. Li, and H. Jiang, Mol. Cryst. Liq. Cryst. **616**, 83 (2015).
[139]Y. Yang, W. Zhan, R. Peng, C. He, X. Pang, D. Shi, T. Jiang, and Z. Lin, Adv. Mater. **27**, 6376 (2015).
[140]C. Wang, K. Sim, J. Chen, H. Kim, Z. Rao, Y. Li, W. Chen, J. Song, R. Verduzco, and C. Yu, Adv. Mater. **30**, 1706695 (2018).
[141]M. Chambers, B. Zalar, M. Remškar, S. Žumer, and H. Finkelmann, Appl. Phys. Lett. **89**, 243116 (2006).
[142]A. Agrawal, H. Chen, H. Kim, B. Zhu, O. Adetiba, A. Miranda, A. Cristian Chipara, P. M. Ajayan, J. G. Jacot, and R. Verduzco, ACS Macro Lett. **5**, 1386 (2016).
[143]M. Wang, Z.-W. Cheng, B. Zuo, X.-M. Chen, S. Huang, and H. Yang, ACS Macro Lett. **9**, 860 (2020).
[144]V. Domenici, B. Zupancic, V. V. Laguta, A. G. Belous, O. I. V'yunov, M. Remskar, and B. T. Zalar, J. Phys. Chem. C **114**, 10782 (2010).
[145]V. Domenici, M. Conradi, M. Remškar, M. Viršek, B. Zupančič, A. Mrzel, M. Chambers, and B. Zalar, J. Mater. Sci. **46**, 3639 (2011).
[146]Z. Wu, L. Liu, P. Cheng, J. Fang, T. Xu, and D. Chen, J. Mater. Chem. C **7**, 14245 (2019).
[147]J. M. Haberl, A. Sánchez-Ferrer, A. M. Mihut, H. Dietsch, A. M. Hirt, and R. Mezzenga, Adv. Funct. Mater. **24**, 3179 (2014).
[148]J. Sun, Y. Wang, W. Liao, and Z. Yang, Small **17**, e2103700 (2021).
[149]L. Yu, R. Peng, G. Rivers, C. Zhang, P. Si, and B. Zhao, J. Mater. Chem. A **8**, 3390 (2020).
[150]Z. Wu, P. Cheng, W. Zhao, J. Fang, T. Xu, and D. Chen, New J. Chem. **44**, 10902 (2020).
[151]C. J. Camargo, H. Campanella, J. E. Marshall, N. Torras, K. Zinoviev, E. M. Terentjev, and J. Esteve, Macromol. Rapid. Commun. **32**, 1953 (2011).
[152]C. J. Camargo, H. Campanella, J. E. Marshall, N. Torras, K. Zinoviev, E. M. Terentjev, and J. Esteve, J. Micromech. Microeng. **22**, 075009 (2012).
[153]N. Torras, K. E. Zinoviev, J. E. Marshall, E. M. Terentjev, and J. Esteve, Appl. Phys. Lett. **99**, 254102 (2011).
[154]M. Wang, S. M. Sayed, L.-X. Guo, B.-P. Lin, X.-Q. Zhang, Y. Sun, and H. Yang, Macromolecules **49**, 663 (2016).
[155]C. Li, Y. Liu, X. Huang, and H. Jiang, Adv. Funct. Mater. **22**, 5166 (2012).
[156]Y. Yang, Z. Pei, Z. Li, Y. Wei, and Y. Ji, J. Am. Chem. Soc. **138**, 2118 (2016).
[157]R. M. Parker, G. Guidetti, C. A. Williams, T. Zhao, A. Narkevicius, S. Vignolini, and B. Frka-Petesic, Adv. Mater. **30**, 1704477 (2018).
[158]J. P. Lagerwall, C. Schütz, M. Salajkova, J. Noh, J. H. Park, G. Scalia, and L. Bergström, NPG Asia Mater. **6**, e80 (2014).
[159]X. M. Dong, T. Kimura, J.-F. Revol, and D. G. Gray, Langmuir **12**, 2076 (1996).
[160]A. G. Dumanli, G. Kamita, J. Landman, H. V. D. Kooij, B. J. Glover, J. J. Baumberg, U. Steiner, and S. Vignolini, Adv. Opt. Mater. **2**, 646 (2014).
[161]A. G. Dumanli, H. M. van der Kooij, G. Kamita, E. Reisner, J. J. Baumberg, U. Steiner, and S. Vignolini, ACS Appl. Mater. Interfaces **6**, 12302 (2014).
[162]A. Tran, W. Y. Hamad, and M. J. MacLachlan, Langmuir **34**, 646 (2018).
[163]O. O'Keeffe, P.-X. Wang, W. Y. Hamad, and M. J. MacLachlan, J. Phys. Chem. Lett. **10**, 278 (2019).
[164]K. Yao, Q. Meng, V. Bulone, and Q. Zhou, Adv. Mater. **29**, 1701323 (2017).
[165]M. Gu, C. Jiang, D. Liu, N. Prempeh, and I. I. Smalyukh, ACS Appl. Mater. Interfaces **8**, 32565 (2016).
[166]R. Bardet, N. Belgacem, and J. Bras, ACS Appl. Mater. Interfaces **7**, 4010 (2015).
[167]H.-S. Park, S.-W. Kang, L. Tortora, S. Kumar, and O. D. Lavrentovich, Langmuir **27**, 4164 (2011).
[168]P. Flory, Macromolecules **11**, 1138 (1978).
[169]M. Xu, W. Li, C. Ma, H. Yu, Y. Wu, Y. Wang, Z. Chen, J. Li, and S. Liu, J. Mater. Chem. C **6**, 5391 (2018).
[170]T. Wu, J. Li, J. Li, S. Ye, J. Wei, and J. Guo, J. Mater. Chem. C **4**, 9687 (2016).
[171]Y. Yang, X. Wang, H. Huang, S. Cui, Y. Chen, X. Wang, and K. Zhang, Adv. Opt. Mater. **8**, 2000547 (2020).
[172]J. A. Kelly, A. M. Shukaliak, C. C. Y. Cheung, K. E. Shopsowitz, W. Y. Hamad, and M. J. MacLachlan, Angew. Chem. Int. Ed. **52**, 8912 (2013).
[173]T. Lu, H. Pan, J. Ma, Y. Li, S. W. Bokhari, X. Jiang, S. Zhu, and D. Zhang, ACS Appl. Mater. Interfaces **9**, 18231 (2017).
[174]C. C. Y. Cheung, M. Giese, J. A. Kelly, W. Y. Hamad, and M. J. MacLachlan, ACS Macro Lett. **2**, 1016 (2013).
[175]E. Lizundia, T.-D. Nguyen, J. L. Vilas, W. Y. Hamad, and M. J. MacLachlan, J. Mater. Chem. A **5**, 19184 (2017).
[176]M. Chau, K. J. De France, B. Kopera, V. R. Machado, S. Rosenfeldt, L. Reyes, K. J. W. Chan, S. Förster, E. D. Cranston, T. Hoare, and E. Kumacheva, Chem. Mater. **28**, 3406 (2016).
[177]Q. Liu and I. I. Smalyukh, Sci. Adv. **3**, e1700981 (2017).
[178]D. Ge, L. Yang, G. Wu, and S. Yang, J. Mater. Chem. C **2**, 4395 (2014).
[179]C. E. Boott, A. Tran, W. Y. Hamad, and M. J. MacLachlan, Angew. Chem. Int. Ed. **59**, 226 (2020).
[180]J. Chen, L. Xu, X. Lin, R. Chen, D. Yu, W. Hong, Z. Zheng, and X. Chen, J. Mater. Chem. C **6**, 7767 (2018).
[181]Y. H. Jung, J. H. Kim, and J. A. Rogers, Adv. Funct. Mater. **30**, 2008805 (2020).
[182]H. Kim, J. Gibson, J. Maeng, M. O. Saed, K. Pimentel, R. T. Rihani, J. J. Pancrazio, S. V. Georgakopoulos, and T. H. Ware, ACS Appl. Mater. Interfaces **11**, 19506 (2019).
[183]D. J. Roach, C. Yuan, X. Kuang, V. C. Li, P. Blake, M. L. Romero, I. Hammel, K. Yu, and H. J. Qi, ACS Appl. Mater. Interfaces **11**, 19514 (2019).
[184]J. S. Gibson, X. Liu, S. V. Georgakopoulos, J. J. Wie, T. H. Ware, and T. J. White, IEEE Access **4**, 2340 (2016).
[185]S. U. Kim, Y. J. Lee, J. Liu, D. S. Kim, H. Wang, and S. Yang, Nat. Mater. **21**(1), 41–46 (2022).
[186]F. Vollrath and D. P. Knight, Nature **410**, 541 (2001).